Radiative Wireless Power Transfer: Where We Are and Where We Want to Go

Radiative Wireless Power Transfer: where we are and where we want to go

Authors:

Valentina Palazzi 1, Ricardo Correia 2, Xiaoqiang Gu 3, Simon Hemour 4, Ke Wu 3, Alessandra Costanzo 5, Diego Masotti 5, Enrico Fazzini 5, Apostolos Georgiadis 6, Hooman Kazemi 7, Ricardo Pereira 2, Naoki Shinohara 8, Dominique Schreurs 9, Jung-Chih Chiao 10, Alexandru Takacs 11, Daniela Dragomirescu 11, Nuno Borges Carvalho 2

1 Department of Engineering, University of Perugia, Perugia, Italy

2 Institute of Telecommunications, University of Aveiro, Aveiro, Portugal

3 Poly-GRAMES Research Center, Department of Electrical Engineering, École Polytechnique de Montréal, Montreal, QC H3T 1J4, Canada

4 IMS Laboratory, CNRS UMR 5218, Bordeaux INP, University of Bordeaux, 33045 Talence, France.

5 Alma Mater Studiorum - University of Bologna, DEI- Department of Electrical, Electronic and Information Engineering “Guglielmo Marconi”, Bologna, Italy

6 The Hague, Netherlands

7 Raytheon Technologies Corporation, Raytheon Intelligence and Space, 2000E El Segundo Blvd, El Segundo, CA 90245, USA

8 Kyoto University,Research Institute for Sustainable Humanosphere,Japan

9 ESAT-WAVECORE Division, University of Leuven, Leuven, Belgium

10 Electrical and Computer Engineering Department, Southern Methodist University (SMU), Dallas, TX 75275 USA

11 LAAS-CNRS, Université de Toulouse, INSA, UPS, Toulouse, France

Scope

Providing energy to Internet of Things apparatuses is ever more challenging. Humans are increasingly invested in the revolutionary new scenario that experts call “Industry 4.0”, where billions of electronic devices are interconnected with one another. The operations of battery charging or battery replacement for these devices will soon become infeasible. As a consequence, radiative wireless power transfer (WPT) will soon become a leading technology, since it is the only method available to support this technological revolution, and several information communication technology (ICT) companies have already begun to actualize their interest in it.

The interest in ultra low power, energy autonomous wireless sensors has been further fuelled by 5th generation (5G) communication systems, consisting of a massive number of interconnected devices communicating at low bit rates [1], and it is expected that the interest in energy autonomous wireless sensing platforms will only continue into the sixth generation (6G) systems and beyond.

This paper aims to address radiative WPT technology, systems, and strategies for the future of this new electrical engineering paradigm.

The function of a radiative WPT system is to use RF signals to power electronic apparatuses which are far from the RF energy source. The RF power propagating in free space is captured by a circuit called a rectenna. The main building components of rectennas are antennas, used to capture the RF power, and rectifiers, responsible for converting the RF power into DC power. Starting from the analysis of the basic components of radiative WPT systems, this paper aims to bring together RF circuit and system designers with different backgrounds to:

1) provide a clear view of the circuit and subsystem solutions to implement radiative WPT;

2) present novel technologies that minimize cost and maximize integration of the electronics with the environment and with the targeted applications; and

3) highlight the potential of WPT solutions to support future electronics evolutions.

The paper benefits from a wide network of experts from both academia and industry that address the existing and upcoming challenges in wireless power transmission scenarios in an interdisciplinary manner, paving the way for future generations of wireless power transmission solutions and the associated regulation.

At present, the power transmission limits and operating frequency bands for radiative WPT systems are not regulated. For WPT systems operating in the ISM band 2.4-2.5 GHz, power transmission must satisfy the EIRP limits (36 dBm in the US, and 27 dBm in Europe [2]). The transmitted power is usually enough to supply ultra-low power IoT devices [3] at a distance of a few meters. Indeed, the power consumption of transponders based on low-cost transmission protocols (such as BLE, or semi-active RFIDs) with low-duty cycle operation is on the order of 1μW-1 mW. In far field, assuming the signal propagates in free space, the power density decreases as the square of the distance, as shown in Fig. 1. Therefore, the maximum distance between the transmitter and the tag is about 10 m. Studies on ultralong-range WPT systems (transmitting a few kWs) have been reported for power-beaming applications as well [4].

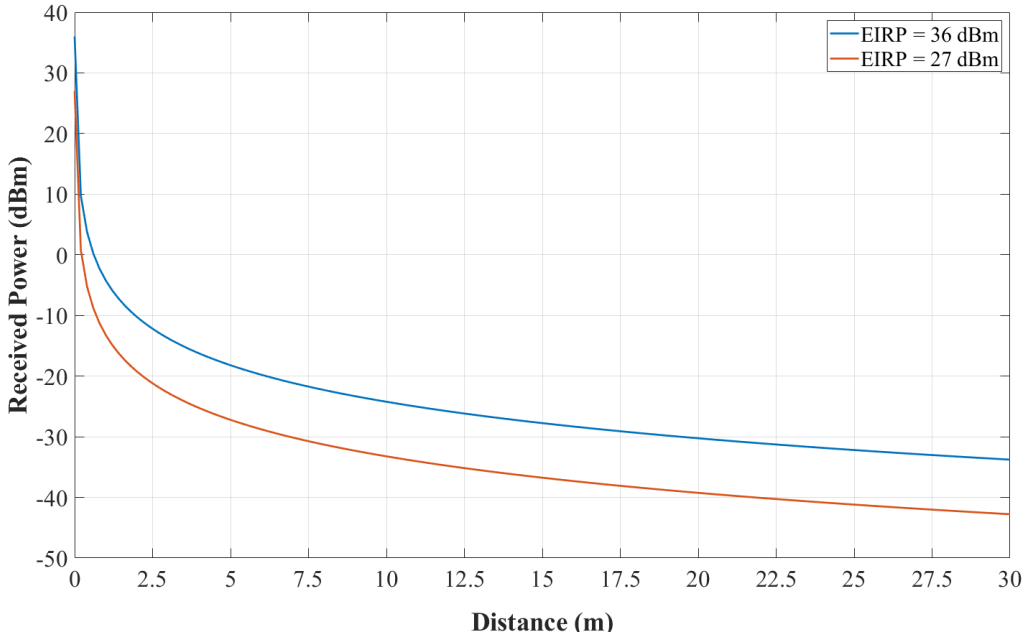

Fig. 1. Received power as a function of the transmitter-to-receiver distance for different values of transmitted power EIRP. Receiver gain equal to 3 dB.

Antennas for WPT

Antennas are one of the key building blocks of radiative WPT systems. They determine how the RF power is transmitted through space, and how it is acquired by the WPT receivers.

Antennas are also the most cumbersome parts of WPT receivers. Therefore, the manufacturing technologies and design approaches adopted for the antenna determine the characteristics of the WPT receiver, in terms of area, weight, flexibility, and robustness.

Radiative WPT systems can be classified based on the type of available energy source, which can be *intentional* or *unintentional*.

In WPT systems with intentional sources, the RF power is transmitted by ad-hoc RF transmitters. This means that the frequency of the RF signal which conveys the power is known. Therefore, narrowband antennas can be used.

If the position of the receivers with respect to the transmitter is also known, high-gain antennas and arrays can be used both to transmit and to receive RF power, if this is allowed by the spatial constraints associated with the application. On the transmitter side, beamforming techniques can be used to shape the radiation pattern, so that the power is transmitted only in the direction of the receivers (closed-loop WPT systems have also been investigated to maximize the output DC power at the receiver side).

If the position of the receivers with respect to the transmitters is unknown, which is true in many applications, omnidirectional radiation patterns are needed. Additionally, circularly or dual polarized antennas can be used to mitigate polarization loss caused by an arbitrary receiver-to-transmitter orientation [5].

In WPT systems with unintentional sources, however, there are no dedicated RF power sources. The receivers harvest the RF power available in the environment. We usually talk of “energy harvesting” (EH) or “energy scavenging” systems. The frequency of the available signals is not usually known in advance. Therefore, broadband and multi-band antennas must be used to cover all relevant bands

used for telecommunications [6], [7]. This is essential to maximize the acquired power in a given scenario, and to improve system reliability. Omnidirectional and circularly polarized antennas are required as well [8]. Rectenna arrays can also be used (in applications with no restrictive spatial constraints) to increase the active area of the WPT receiver [9] [3], where each antenna is equipped with its own rectifier. This way, the received power is rectified by each element independently, and the obtained DC power is finally summed.

Antennas for WPT systems can be either matched to 50 Ohm or directly to the input impedance of the rectifier. With the latter approach, the input matching network between the rectifier and the antenna can be avoided, thereby reducing the rectenna complexity, losses, and area [10]. Nevertheless, this makes the antenna design more challenging (the input impedance of the rectifier for low available input powers has a significant capacitive component and a small real part). Usually dipole antennas with T-matching networks are used for this purpose. Additionally, the antenna and the rectifier cannot be tested separately. Therefore, this solution can be adopted only if the component models and the adopted manufacturing technologies are mature.

Planar microstrip antennas such as rectangular patches are mostly chosen for WPT receivers used in wearable applications [11], [12]. The presence of a ground plane reduces the impact of the human body on the antenna performance. Thick fabrics are used to improve the system efficiency.

As WPT receivers can be used to power sensors placed on common items, flexible antennas can be used to conform the circuit to the object. In this case, wire and slot antennas are preferred, since thin substrates usually do not allow for efficient microstrip antenna solutions in the sub-6 GHz spectrum.

In Fig. 2 two flexible multi-band rectennas are shown [7], [13]. The solution in Fig. 2 (a) is based on two nested annular slot antennas matched to 50 Ohm in the bands 790-960 MHz and 1.71–2.69 GHz, while the solution in Fig. 2 (b) is based on a Yagi-Uda antenna directly matched to the input impedance of the rectifier at the two operating frequencies (915 MHz and 2.45 GHz).

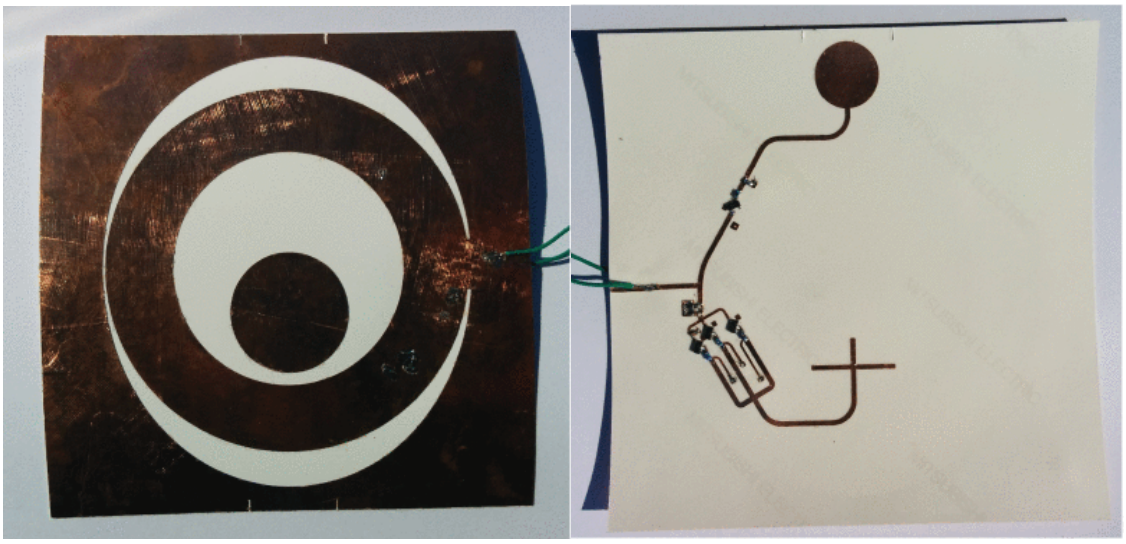

(a)

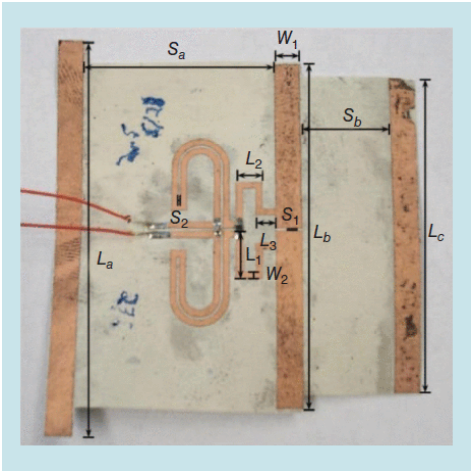

(b)

Fig. 2. Examples of flexible rectennas. (a) multiband rectenna based on two nested annular slots [7], and (b) dual-band rectenna based on a Yagi-Uda antenna [13].

3D printed antennas and 3D antenna arrays have been also investigated [14], to allow WPT receivers to harvest energy from different directions (see for instance Fig. 3).

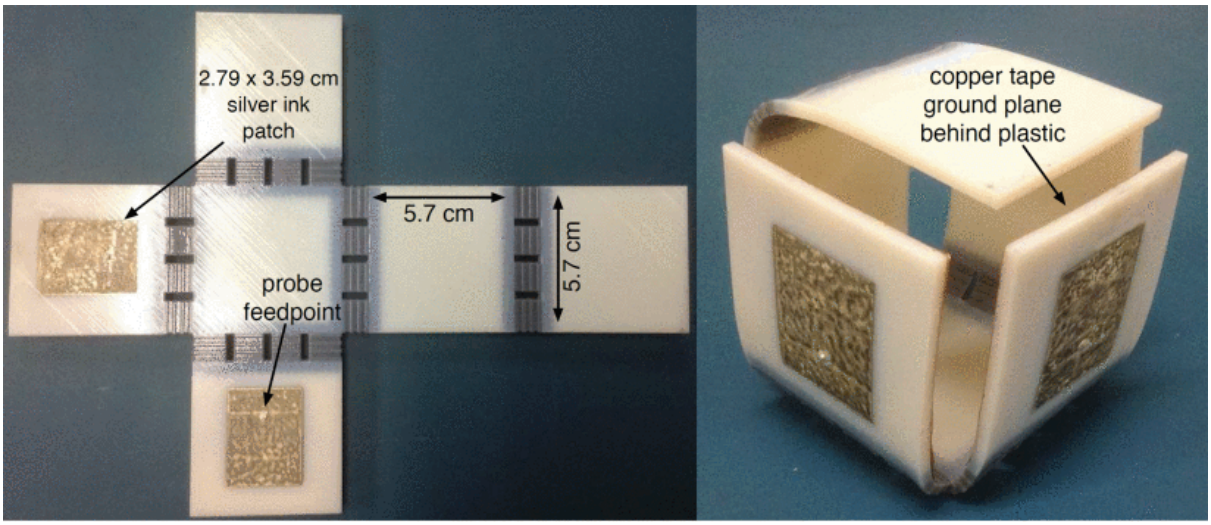

Fig. 3. Example of 3D printed antenna for RF energy harvesting [14].

RF-DC converters

RF-DC converters are RF circuits that convert RF signals back to DC voltage. They are normally composed of a matching network (to allow the maximum power transfer between the antenna and the nonlinear rectifier), a nonlinear rectifying device, and a low-pass filter that is then connected to a load or to a current source.

Usually, the nonlinear rectifying device is a Schottky diode, due to its low-voltage threshold and low-junction capacitance, which results in a more efficient operation at low powers and in a higher maximum operation frequency.

Fig. 4 presents the RF-DC conversion efficiency of different rectifiers with different topologies from 450 MHz to 94 GHz, based on [15]. Besides the single-band converters presented in Fig. 4, dual-band

converters that are able to convert RF power from two different transmitter sources are presented in [16], and a triple-band converter is presented in [17].

Most traditional rectifiers can only exhibit reasonable RF-DC conversion efficiency with a narrow input power range. The efficiency declines severely when the input power deviates from the operating range, limiting the wireless charging applications with considerable variations of input power. Thus, it is necessary to implement and design rectifiers with a wide operating input power range [18], [19], [20]. The authors in [21] designed an adaptive rectifier for WPT which can adapt the configuration of the rectifier to the input power level.

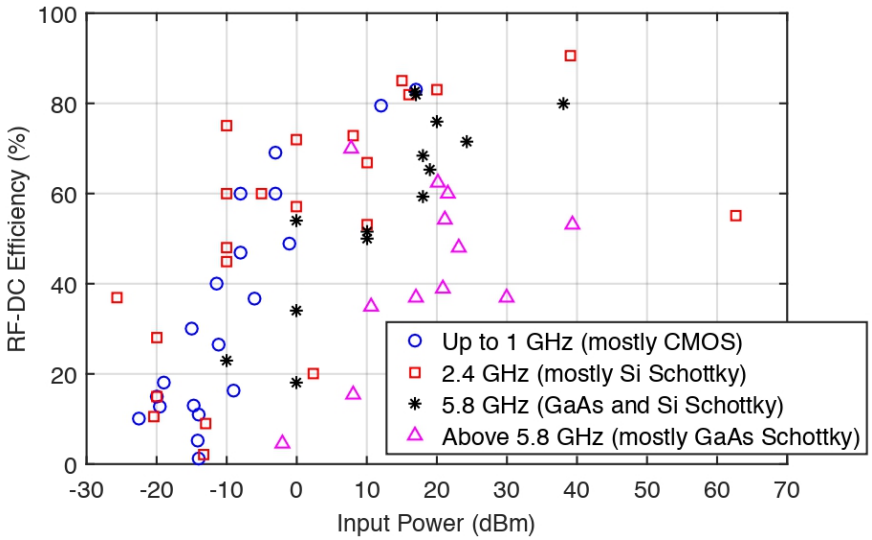

Fig. 4. State of the art in RF-DC converters, with different topologies, from 450 MHz to 94 GHz.

In Fig. 5 different topologies of rectifiers are presented. Charge pumps (voltage multipliers) are the most used in RFID applications, since they require a considerable DC voltage to power electronics. The main conclusions that can be taken from simulations and experimental work are:

- The efficiency of the rectifier decreases with an increase in the number of diodes (increasing the number of diodes means increasing the parasitics, fewer diodes means a lower amount of input power is necessary to switch on the rectifying devices) and
- Increasing the number of stages will increase the output voltage.

Most of the circuits for WPT applications are based on diode solutions and are optimized for low-power RF signals [22], [23]. High-efficiency rectifiers for a few watts of input power have been studied as well [24], [25]. If the main objective is the use of these RF-DC converters in very high power configurations, then transistor-based RF-DC converters can be used.

The efficiencies of rectifiers are very low for lower input powers. Some authors have addressed this problem in diode-based solutions, including [26], [27], which showed that the RF-DC conversion efficiency can be improved by selecting the appropriate excitation signal. In [28] the use of multitone signals was proposed to increase the efficiency in RF-DC converters with Schottky diodes. In [29] the use of chaotic signals was proposed to increase RF-DC conversion efficiency for EH systems as well as for WPT. The authors in [29] used the Schottky diode approach to implement the rectifier. The use of high peak-to-average power ratio (PAPR) waveforms (intermittent CW signals by varying the duty-cycle, UWB signals, power-optimized waveforms (POW), chaotic signals, white noise, modulated

signals, and multi-carrier signals) to increase and improve the WPT efficiency has been demonstrated in [26]-[31]. Some more recent work focuses on the model to enable an analysis of a multisine-based WPT system focusing on the bandwidth of the signal and the rectifier [32]. The authors in [33] demonstrated the use of modulated signals to improve the RF-DC converter efficiency. They proposed instantaneous power variance (IPV) to describe, more accurately than PAPR, the variation of the instantaneous power and the occurrence of signal peaks that directly affect the RF-DC converter efficiency.

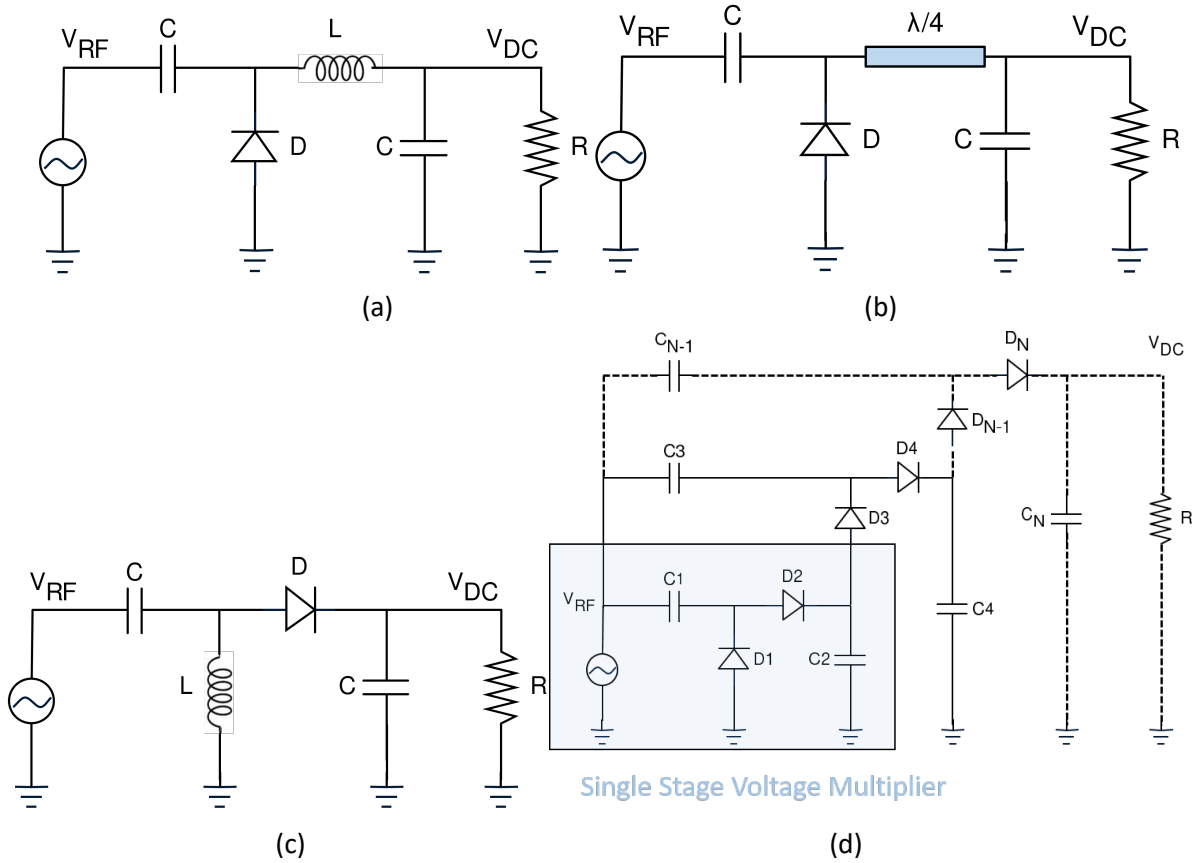

Fig. 5. Different rectifier topologies. (a) Series diode rectifier. (b) Shunt diode rectifier. (c) Shunt diode with $\lambda/4$ stub. (d) N-stage Dickson voltage multiplier.

Diode modeling of low-power rectifiers

Since the difference in the diode nonlinear junction resistance under forward and reverse biases is not substantial for low input power, the Shockley diode model is adopted instead of the commonly used ON-OFF switch model to develop an efficiency chain for Schottky diode-based low-power rectifiers [34]. Fig. 6(a) shows the equivalent circuit model of a typical low-power rectifier containing four parts: RF input source, matching network, diode, and resistive loading. The matching network removes the influence of diode packaging inductance L_p and capacitance C_p. Thus, the rectifier efficiency η can be described as below, focusing on the Schottky diode itself [35]:

$$\eta = \eta_{RF\_dc} \cdot \eta_p \cdot \eta_{tr} \quad (1)$$

in which:

diode RF-DC conversion efficiency: $\eta_{RF\_dc} = \frac{P_{in} \cdot R_I^2 \cdot R_j^2}{R_l + R_s + R_j}$ (2a)

diode parasitic efficiency: $\eta_p = \left(\frac{1}{1 + (\omega \cdot C_j)^2 \cdot R_s \cdot R_j} \right)^2$ (2b)

source-load DC transfer efficiency: $\eta_{tr} = \frac{R_l}{R_l + R_s + R_j}$ (2c)

where P_{in} is RF input power; R_I is current responsivity, a factor measuring a diode's nonlinearity; and R_s, R_j, and C_j are the series resistance, nonlinear junction resistance, and junction capacitance of the diode. ω and R_l are angular frequency and load resistance.

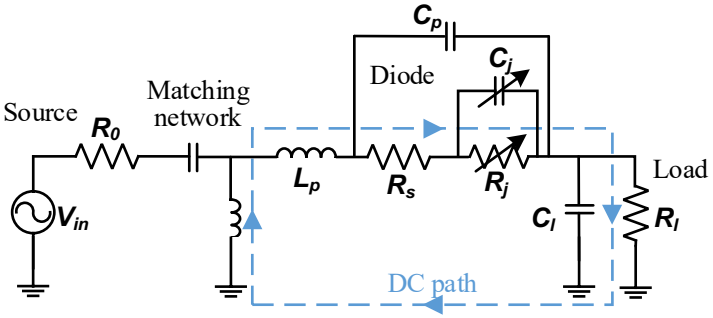

(a)

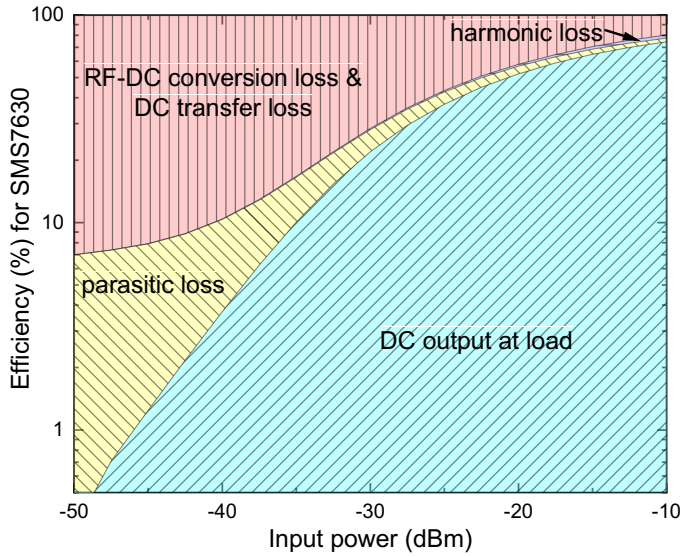

(b)

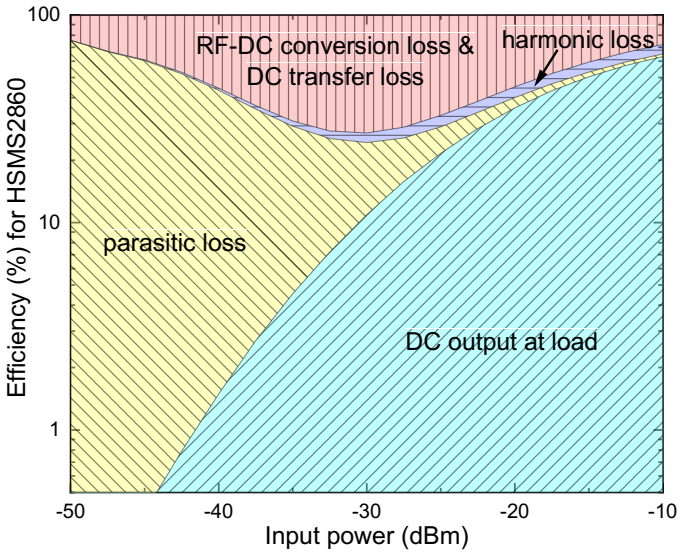

(c)

Fig. 6. (a) Equivalent circuit of a typical Schottky diode-based low-power rectifier. Rectifier efficiency for (b) SMS7630 and (c) HSMS2860 against an input power range of −50 dBm to −10 dBm, where load resistance is 5.4 kΩ and operating frequency is 0.9 GHz.

Diode RF-DC conversion efficiency η_{RF-DC} is only associated with nonlinear junction resistance R_j as only R_j supports a DC path, as shown in Fig. 6(a). Also, (2a) indicates that higher RF input power P_{in}, stronger diode nonlinearity R_I, and larger diode junction resistance R_j all drive up η_{RF-DC}. Diode parasitic efficiency η_p characterizes the amount of RF power going through C_j and eventually dissipated by R_s eventually. A smaller junction capacitance C_j and series resistance R_s can help leverage η_p, according to (2b). Finally, source-load DC transfer efficiency η_{tr} quantifies how much DC power arrives at R_l, which can be calculated by the voltage divider rule in (2c). The optimum load resistance R_l can be approximated as $R_j + R_s$ based on (2c).

The above analysis is suitable for understanding the loss (efficiency) mechanism of Schottky diode-based low-power rectifiers with explicit formulae. Zero-bias values R_{j0} and C_{j0} are generally adopted in the analysis. However, R_j and C_j vary under different input power levels. Therefore, the above analysis is valid in a limited power range (< −35 dBm). An analytical model is then developed to extend the dynamic range of accurate prediction for rectifiers' power conversion efficiency (PCE). The PCE can be defined as [36]:

$$\eta_{PCE} = \frac{P_{DC}}{P_{in}} \times 100\% = \frac{P_{DC}}{P_{R_j}+P_{R_s}} \times 100\% \tag{3}$$

where the DC output power P_{DC} can be calculated by the generated DC current multiplying the load resistance $I_{DC}^2 \cdot R_l$. The RF input power P_{in} contains two parts: the power absorbed by R_j (P_{R_j}) and consumed by R_s (P_{R_s}). Considering the voltage-controlled current (I) − voltage (V) relation of R_j and capacitance (C) − voltage (V) relation of C_j, the generated DC current I_{DC} and RF input power P_{in} can be calculated with better accuracy. Hence, the dynamic range of this model for PCE prediction can be extended to −10 dBm, which is enough for ambient RF energy rectifier analysis.

As one example, Fig. 6(b) and (c) demonstrate the rectifier conversion efficiency and loss mechanism for two diodes: SMS7630 and HSMS2860, respectively. From the comparison, SMS7630 is clearly a better candidate for low-power rectifier design as it delivers higher efficiency throughout the entire power range. When the input power increases, parasitic loss tends to reduce due to a smaller effective R_j, while harmonic loss has an opposite tendency. Regarding the HSMS2860 diode, its large junction resistance R_j (due to a small saturation current I_s) offers smaller RF-DC conversion loss and source-load DC transfer loss at a low power level. However, a large R_j brings significant parasitic loss, as seen in Fig. 6(c).

Smart RF and mm-Wave Showers

In far-field WPT, the power is exchanged by radiative electromagnetic (EM) waves, allowing us to cover long distance links and typically involving low levels of power. The most important figure of merit in this scenario is the efficiency:

$$\eta_{LINK} = \eta_{TX}\,\eta_{FS}\eta_{RX} = \frac{P_{TX}}{P_{BIAS}}\frac{P_{RX}}{P_{TX}}\frac{P_{DC}}{P_{RX}} \tag{4}$$

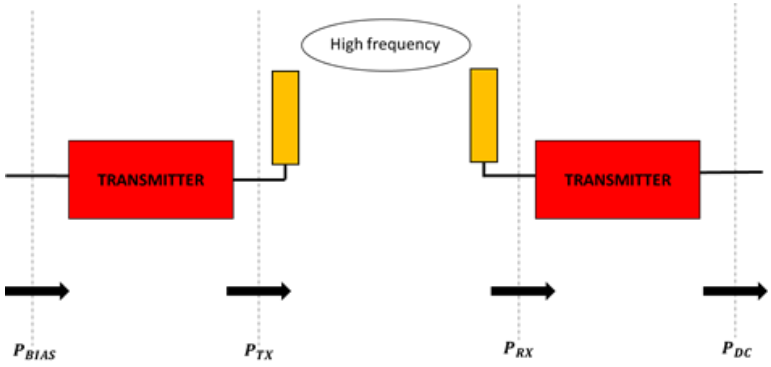

Fig. 7. Far-field WPT block schematic and the efficiency contribution

Within the three main efficiencies involved, as shown in Fig. 7, the TX and the RX efficiencies (η_{TX} and η_{RX} , respectively) have almost reached their upper limits. The main bottleneck is represented by the transmission efficiency in free space, η_{FS} , because only a small amount of the transmitted power actually reaches the receiver location, and this causes a drop in the overall system performance, mainly because the attenuation makes the power decrease rapidly after a few meters. The solution is offered by the so-called “Smart RF” or “mm-wave showers,” illuminators that are able to provide a high level of reconfigurability in real time under demanding power-control conditions [37]. Here, two technologies are reported that are aimed at improving η_{FS}, both of which leverage the concept of diversity in its two guises: frequency diversity applied by frequency-diverse arrays (FDAs) and time diversity applied by time-modulated arrays (TMAs).

In frequency diverse arrays, each radiating element radiates with a frequency slightly different from its neighbors. The result, given by the intermodulation of the different tones, allows us to dynamically compose an array factor (AF) that, for a fixed instant, is able to provide energy in real time not only in prescribed directions, but also at a prescribed distance from the transmitting source. In this way, the transmitted power can be concentrated at desired spots, and can be drastically reduced in undesired ones, with the twofold advantage of increasing energy efficiency where it is needed and minimizing the power where it is not needed. After several studies on the characteristics of traditional linear FDAs,

attention has moved to improving the focusing capabilities of these radiating architectures: planar bi-dimensional array arrangement has been identified as an answer to this requirement. The multi-finger frequency diverse array belongs to this family, where the array is arranged as a tree with M radiating elements aligned along the x-axis and N along the y-axis. An example of the layout and its astonishing properties are presented in Fig. 8, which highlights the availability of a planar array configuration which allows us to improve the focusing capability with respect to a linear FDA, reducing the area of the spot in the θ direction, while the "S-shape" of the beam pattern is still present, as can be seen in Fig. 8(c). This shows the main limitation of FDAs: the displacement in time of the main beam. This means that, as time passes, the power is not fixed and moves farther away from the source periodically with a period equal to the inverse of the frequency increment applied to two consecutive elements or groups of elements.

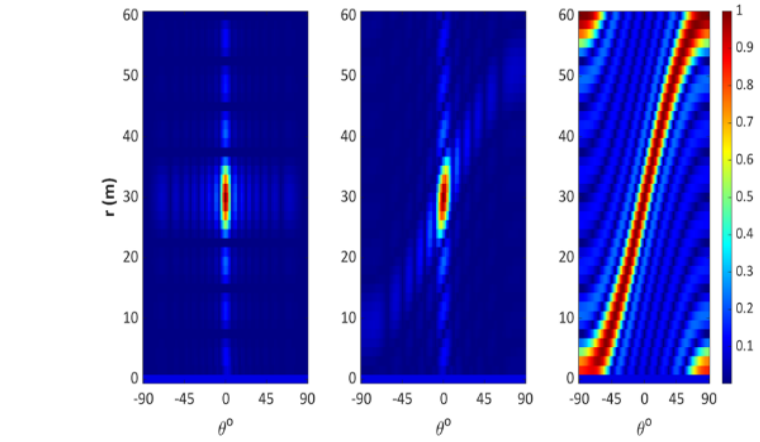

Fig. 8. Normalized BP of the standard FDA for t = 100 ns: (a) in the plane (r, q, f=90°); (b) in the plane (r, q, f=45°); (c) in the plane (r, q, f=0°); (d) Normalized BP in the (t, r, θ = 0°,f=0°) space; and (e) Planar array in "tree" configuration operating at 24 GHz, with M=8 "branches" and N=16 series-fed patch antennas.

Several techniques have been proposed to counterbalance this undesired effect for WPT, and the most promising one is called time-controlled frequency diverse arrays (TCFDA). Each input signal is modulated by a periodic pulse presenting two new design parameters: the first one able to intercept

the power at a desired distance from the source, and the second one to define the coverage area. As a consequence of the application of this time-based technique, the power can be fixed at a certain distance from the transmitting source and drastically reduced in undesired regions, as can be seen in the examples shown in Fig. 9.

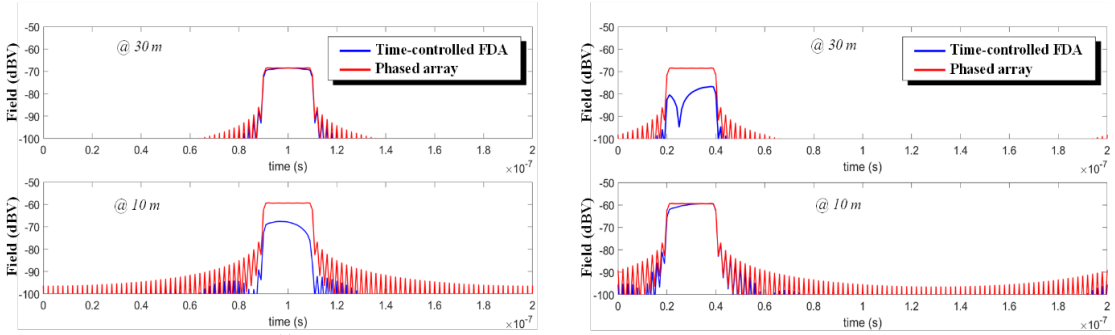

Fig. 9. (a) BP (accounting for isotropic attenuation) vs. time when the TCFDA is designed to focus at (r, θ, ϕ) = (30 m, 0°, 0°). (b) BP (accounting for isotropic attenuation) vs. time when the TCFDA is designed to focus at (r, θ, ϕ) = (10 m, 0°, 0°).

The proposed design highlights the great potential of FDAs for selective far-field WPT "on-the-move" applications.

Time modulated arrays (TMAs), first introduced in the 1950s, have recently garnered increased interest due to exponential electronic development that is able to produce and sustain the time-diversity concept: in a linear array with high-performance RF switches driven by precise control sequences, a simultaneous multi-frequency radiation can be exploited to allow it to point the many beams in different directions at the same time. The almost unlimited number of driving sequences leads to manifold benefits: sidelobe suppression relaxing the array design constraint, electronic beam scanning through the generation of multiple beams pointing at different angles without the use of phase shifters, and finally an important reduction in the system cost. The schematic representation and the multi-harmonic radiation mechanism of a TMA are presented in Fig. 10.

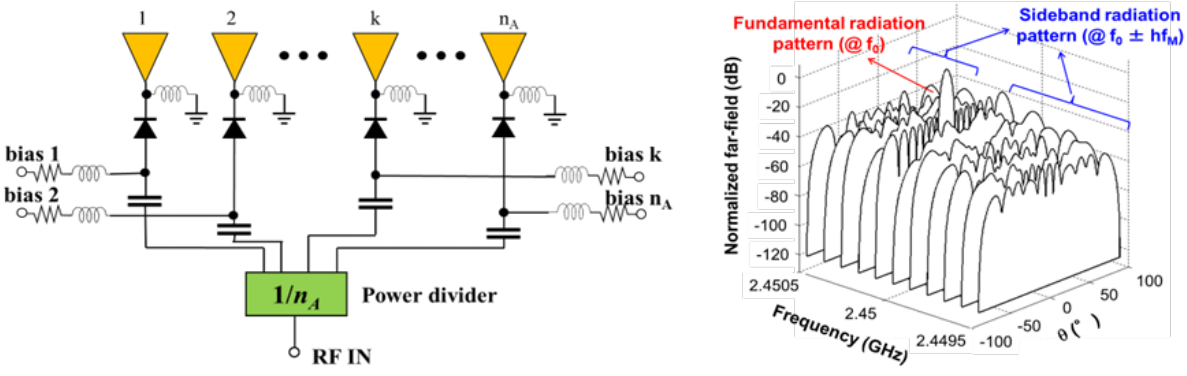

Fig. 10. (Left) Schematic representation of a linear, n-element TMA, with detailed diode switch bias networks, including DC-block capacitors, (Right) Multi-frequency radiation patterns of a 16-element linear TMA.

In WPT applications this technology represents one of the most promising solutions for simultaneous energization of objects located in different positions [38]. The main concern is the synthesis of the optimum sequence for the driving of the RF switches, in order to fully leverage the time diversity

capability. As an expression of this great potential, Fig. 11 shows both the ON-OFF sequence of 16 switches of a 16-element linear array operating at f0=2.45 GHz, and the corresponding simultaneous radiation patterns involving the fundamental carrier and its upper and lower sideband harmonics (f0±fM=2.45 GHz ± 100 kHz, in this case).

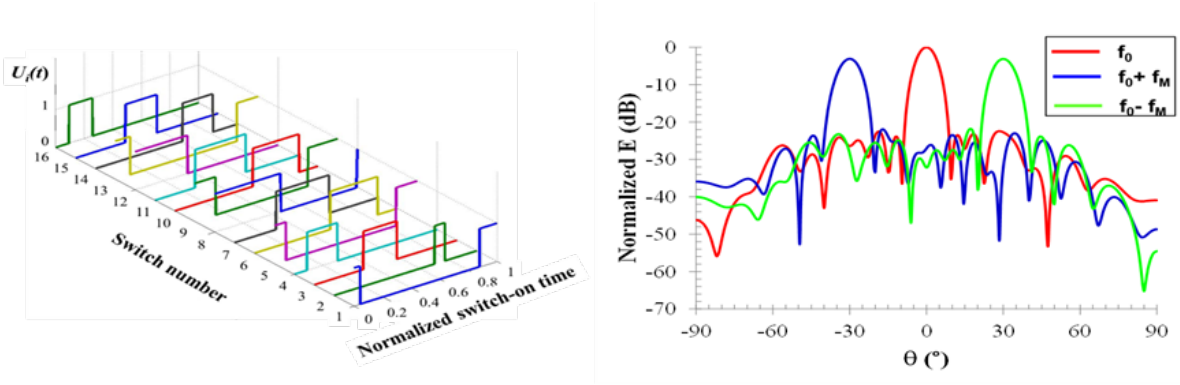

Fig. 11. (Left) Switches control pattern optimized for WPT purposes, for a 16-monopole array. (Right) Radiation patterns at the fundamental and at the two first symmetrical sideband harmonics

These promising results, obtained by means of the simple architecture implementation shown in Fig. 10, indicate that TMAs are potential candidates for agile and reconfigurable WPT systems, to be exploited in many civil and industrial scenarios.

Quasioptics and its use in WPT

Beam propagation is associated with one of the major problems in WPT, spillover losses (see Fig. 12). These happen whenever the emitted radiation misses its target, mainly due to the microwave's divergence but also due to system misalignments.

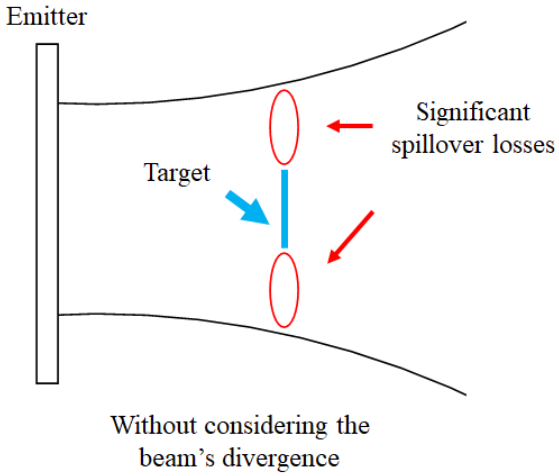

Fig. 12. Microwave beam in a traditional WPT system. The beam's divergence reduces the amount of energy reaching the target.

Antennas' far-field and associated tools are traditionally used in WPT. However, these do not provide us with the means to reduce, or even account for, the spillover losses. In order to do that, a new approach to the radiation's study can be pursued, one that remains practical but is capable of analyzing the microwave's radiation in a more comprehensive manner, so that the beam's divergence is understood and controlled.

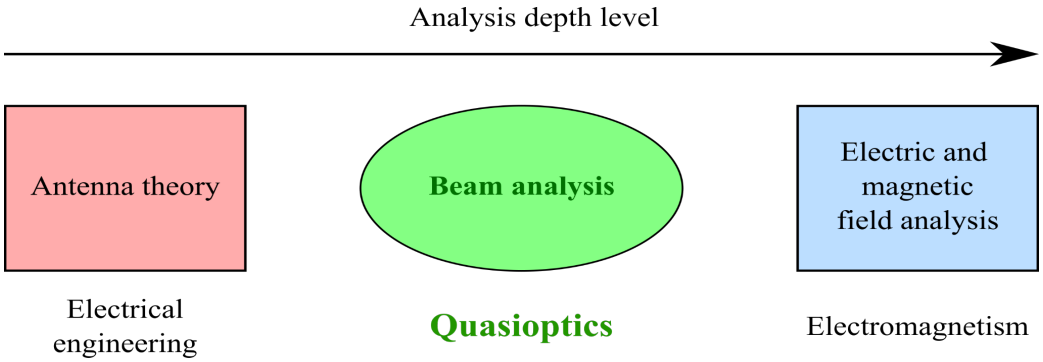

Fig. 13. Different theoretical frameworks for analyzing electromagnetic radiation and radiative wireless power transfer, ordered according to the depth of their analysis. Quasioptics is proposed as the one that best balances implementation difficulty with analysis depth.

Quasioptics appears to be the theoretical framework of choice for the previously mentioned requirements by approximating the emitted EM radiation with Gaussian beams [39]. These flexible mathematical entities are the building blocks of the complete theory, providing information on beam propagation throughout any system (see Fig. 13). The electric field distribution of a Gaussian beam in the fundamental mode, propagating in the $\hat{z}$ direction is given by:

$$E(r,z) = \sqrt{\frac{2}{\pi\varpi^2}}exp\left(-\frac{r^2}{\varpi^2} - ikz - \frac{i\pi r^2}{\lambda R} + i\phi_0\right), \quad (5)$$

where ϖ is the beam radius, the most important parameter for wireless power transfer, since it provides information about the beam's divergence. It is defined as the radial distance at which the power falls to 1/e of the on-axis value (e is Euler's number). The point where the power is most concentrated is given by z_0, and the beam radius is at its minimum at this point; it is called the beam waist, $\varpi_0{}^2$. The electric field varies with the distance to this point, z, and the distance from the axis of propagation, r. Finally, R is the wavefront's radius of curvature, ϕ_0 is the phase shift and λ is the beam's wavelength.

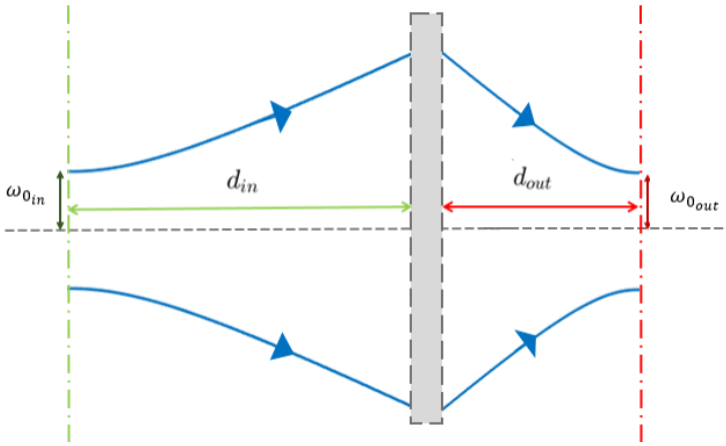

Fig. 14. In this schematic, a quasioptical system transforms an input beam to a thin ray, similar to an optical system. The beam's divergence can therefore be accounted for, potentially reducing spillover losses. The distance from the input to the output beams in the quasioptical system is given by d_{in} and d_{out}, respectively.

With it, the matrix formalism of optics can be used in contexts of significant divergence, as is the case of microwaves travelling distances of meters and kilometers, in order to transform and optimize the beam to the system requirements (Fig. 14). While being mostly used in RF and mmWave astronomy, its application in wireless power transfer systems may be paramount to reducing spillover losses, contributing to an overall increase in efficiency [40]-[42].

Hybrid Energy Harvesting

Energy harvesting is a very broad and diverse field, given that each energy harvesting technology defines a completely different field of research [43].
The physics behind energy harvesting technologies such as solar, mechanical, thermal, and RF have been known for decades-even centuries. More than one hundred years ago, Tesla envisioned the wireless transmission of power. Advances in materials and fabrication techniques such as additive manufacturing have enabled the miniaturization, reduction of cost, and the performance improvement of energy harvesting devices, making them suitable for low power wireless sensors. With advances in electronic design and integrated circuit technologies which have led to further reductions in the operating power and cost of electronic circuits, wireless sensor platforms that are powered by energy harvesting are becoming more and more feasible.

Table I presents some indicative performance from various types of energy harvesters suitable for micro-power generation. There is a large variation among the size of the transducers and the amount of energy that can be generated. As a result, transducer selection depends on the application requirements and scenario, which makes the presented results of Table I only indicative of the potential of the various harvesting methods.

Energy Source	Harvested Power (indicative)	Conditions, Available Power
Light / Solar	60 mW	6 cm x 4 cm a-Si solar cell AM1.5 (100 mW/cm^2)

Kinetic	8.4 mW	Piezoelectric, shoe mounted
Thermal	0.52 mW	TEG, DT = 5.6 K
EM	1.5 μW	Ambient power S = 0.15 $\mu W/cm^2$

Table I. Harvested power potential from different transducer types [44].

Each transducer technology has distinct advantages and disadvantages, and is thus suitable for different application scenarios. One characteristic of ambient energy which makes the design and use of harvesting circuits particularly challenging is its variable and probabilistic nature. A particular challenge is the efficiency of the transducer device itself, which is typically limited and/or strongly dependent on the available input energy and output load. For example, the availability of light energy is reduced in indoor scenarios or at night; thermal energy harvesters are limited by a low maximum transducer efficiency, depending on the existing temperature gradient; while kinetic energy harvesters are sensitive to the natural vibration frequencies of the harvester and application settings. Finally, the available EM energy density is usually orders of magnitude below the corresponding values of the other energy sources, although measurements in urban settings have demonstrated the possibility of harvesting a useful amount of EM energy using wideband or multi-band harvesters [45]-[47]. However, the highly variable nature of ambient energy availability gives rise to application scenarios where EM energy harvesting is justified. One characteristic example is the variation of solar light energy between daytime and nighttime. A second example is placement of sensors sufficiently near transmitting RF base station antennas where RF energy levels may exceed the typical values.

The different energy sources can be combined in a variety of ways. The signal combination can be done at the input or the output of the diode rectifier circuits (i.e., in DC or AC signal form) [43]. Furthermore, the DC signal combination can be done in series or in parallel, resulting in a different optimum load value corresponding to a maximum efficiency. For example, the various signals of RF energy harvesters may be combined in the RF stages before they are fed to the rectifier circuit, resulting in a directive antenna system. Alternatively, the DC outputs of different rectennas can be combined in series or in parallel [48]. Every topology has different advantages and requires a careful design in order to optimize the DC conversion efficiency for a given output load and for the desired input power ranges.

In order to address the aforementioned challenges associated with ambient energy availability, we highlight efforts toward hybrid multi-technology harvesters in the next section [43], [49].

Example multi-technology circuit implementations include a solar-thermal-electromagnetic energy harvester based on a patch antenna integrating a solar cell and a thermoelectric generator [50]. A preliminary prototype is shown in Fig. 15 [50]. The concept of using solar power as an auxiliary power source in order to power-up passive RFID tags has been proposed in [51]. A different implementation of a solar energy-assisted passive RFID tag where the DC power from a solar cell is converted to RF using an oscillator and then fed to the RF pins of a commercial passive UHF RFID tag is shown in Fig. 16 [52]. Finally, ambient backscattering has been proposed as an ultra low-power communication technique where information from an ultra low-power sensor tag is superimposed on existing ambient signals [53]. A low-cost ambient backscatter platform based on commercial off-the-shelf components based on ambient FM station backscattering is shown in Fig. 17 [54]. The potential of combining

ambient backscattering with multiple energy harvesting technologies may further expand the concept of batteryless, “zero power” sensors.

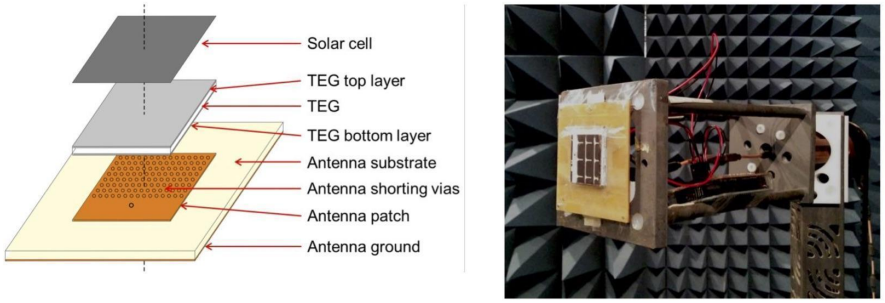

Fig. 15. A stacked configuration of a patch antenna, a solar cell, and a thermoelectric generator for energy harvesting [50].

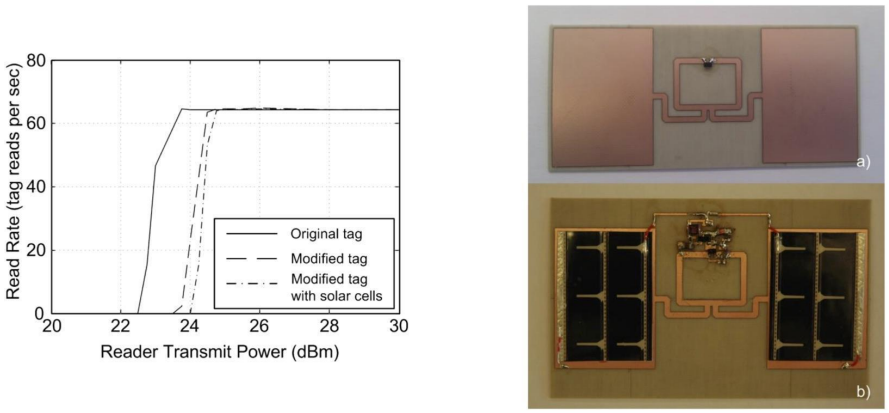

Fig. 16. A solar power-enhanced passive UHF RFID tag [52]. (Left) read rate performance measurement, (Right) a) tag without solar cell, b) tag with integrated solar cell.

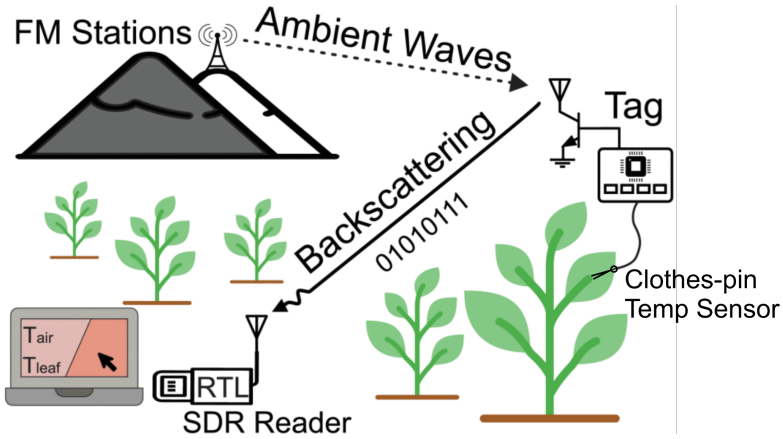

Fig. 17. Ambient backscattering of FM signals [54].

Millimeter-wave Radiative Wireless Power Transmission

Millimeter-wave (mmW) frequencies provide key advantages in radiative WPT applications, such as compactness and focused energy that can be delivered to a target at range with a smaller rectenna surface. Another major advantage of the mmW frequency range is fewer regulatory restrictions for transmission of signals in populated areas compared to the congested 2.45 GHz and 5.8 GHz frequency bands.

Fig. 18 represents the antenna beamwidth and spot size at 1 km distance as a function of transmitter frequency for three transmitter aperture sizes. As the transmitter frequency is increased from the RF to the mmW frequency range, the antenna beamwidth narrows, leading to a smaller spot size on target. This allows for a focused beam of the radiated energy with less spreading loss, while the spot size is not as small as optical beams where pointing and tracking is required, thereby reducing the complexity of the rectenna-based receivers.

Fig. 19 represents the plot of the total RF and mmW power received at the receive antenna as a function of range. For a fixed aperture comparison between the various operating frequencies, the mmW approach is the best performing due to its increased power received at all ranges. The power delivered on target due to the focused beam and higher power density can either manifest itself into a smaller size and weight of a power beaming system or a reduced overall cost for watts delivered at range compared to RF and microwave beaming systems. Advance in high-power MMIC amplifiers in GaN technology as well as high power-density 3D packaging, together with commercial and defense application pulls, will promote the cost effectiveness of millimeter wave power systems in the near future.

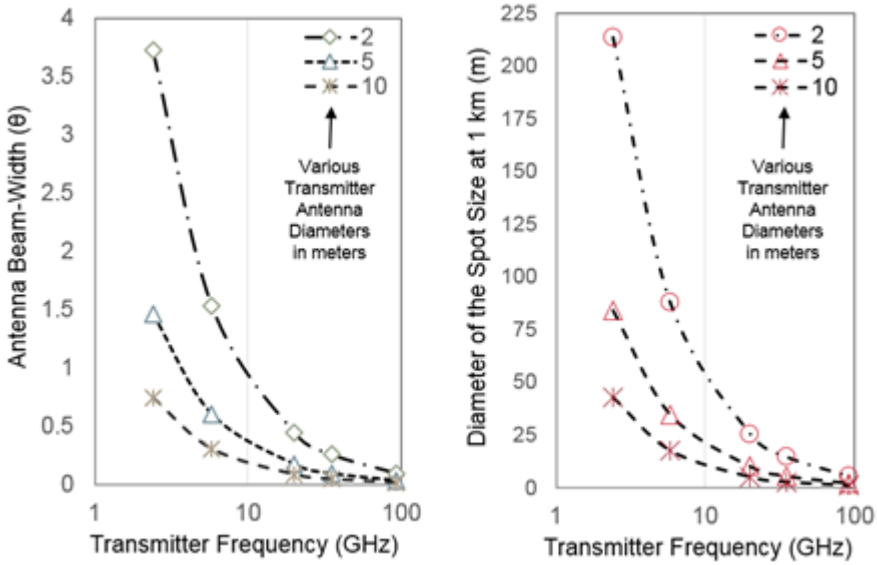

(a) (b)

Fig. 18. RF and mmW WPT system analysis, highlighting antenna beam widths and spot sizes as a function of transmitter frequencies for three transmitter antenna aperture sizes.

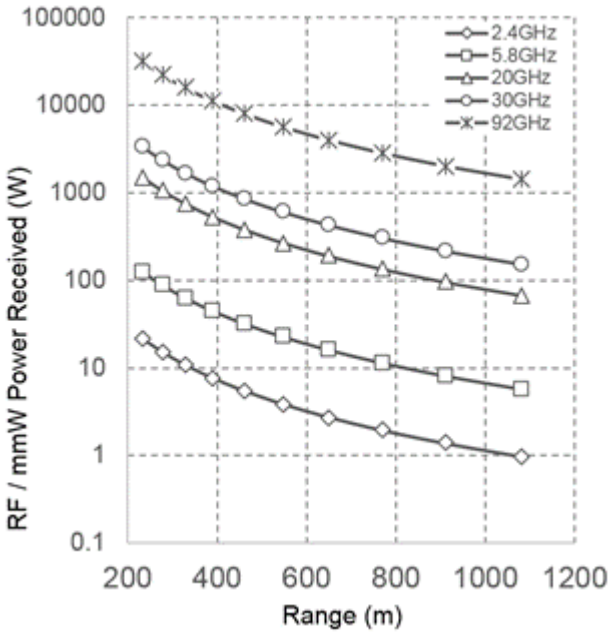

Fig. 19. Received DC power at the rectenna as a function of range for five RF and mmW WPT systems. All transmitter powers are at 100kW with transmit and receive aperture sizes being 2m and 1m in diameter respectively.

The high-power regime for WPT requires a high power handling rectifier diode in order to handle the high incoming radiation at W/cm^2 input power levels. The current device technologies used for wireless power rectification at mmWaves are GaAs and CMOS. The key to high efficiency RF-DC rectification is the high switching speed of the diode (high cut-off frequency) which entails a low series resistance and low associated capacitance. For high-power operation, high forward current handling and reverse breakdown voltage are required. GaAs planar air bridged diodes and CMOS transistors are characterized by high cut-off frequencies. However, their breakdown voltage is limited. For high power operation, a high breakdown voltage is required, moving the choice of technology towards GaN; much like in transistor-based power amplifier integrated circuits with high output power density. Various GaN Schottky diodes have been developed, highlighting the improvement in output rectified power. However, the higher frequency of operation has been limited by the device design and its fabrication process. Fig. 20 illustrates a technology cross-section of the nano-Schottky diode (NSD).

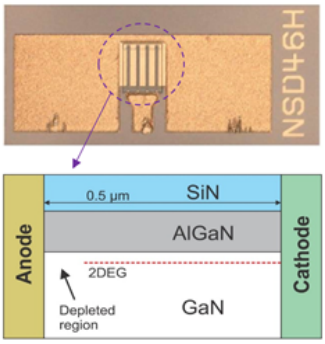

Fig.20. Technology cross-section of the nano-Schottky diode (NSD). The anode metal contacts laterally with a two-dimensional electron gas (2DEG) formed in an AlGaN/GaN HEMT structure. The cathode is made of a regrown n+GaN on the 2DEG.

The epitaxial structure consists of an AlGaN/GaN HEMT structure where a two-dimensional gas (2DEG) is formed near the AlGaN/GaN interface. The sheet electron density and the mobility of the 2DEG are 1.2×1013 cm^2 and 1600 cm^2/V·s, respectively. The 2DEG is confined in the GaN channel layer within a few nanometers below the interface, enabling a nano-scale Schottky contact between the anode metal and the 2DEG. The small Schottky contact area and a lateral depletion length of the 2DEG determine the junction capacitance (Cj). The cathode ohmic contact is formed by an n+GaN layer regrown on the 2DEG. The low contact resistance (= 0.1 W·mm) and the low sheet resistance of the 2DEG (= 330 W/sq.) contribute to a low series resistance (Rs) of the diode. The distance between the anode and the cathode is 0.5 µm. The GaN nano-Schottky diode rectifier was used to design a variety of rectenna circuits for performance evaluation of the developed technology. Fig. 21 shows a voltage doubler rectifier fabricated as an integrated circuit directly on the GaN/SiC wafer using two 2x2x10 µm diodes. The circuit includes an input low-pass filter using a double-stub matching network designed for roll off at 96 GHz, which prevents any higher harmonics power generated by the rectifier to be radiated out of the input port. Similarly, a large integrated thin-film capacitor connected through a substrate via has a low-loss RF short circuit, allowing only DC to be extracted at the output port. An integrated thin film capacitor of value 350 fF was also used for the voltage doubler for charging and discharging operation during forward and reverse operation RF input swing across the rectifier diodes.

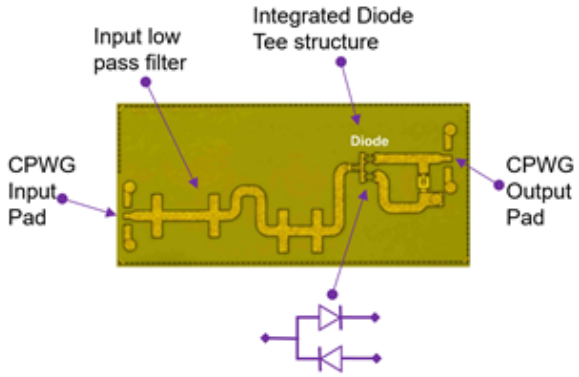

Fig.21. GaN nano-Schottky rectenna MMIC integrated with a voltage doubler diode topology, input LPF, and DC circuitry measuring 2.1mm by 0.75mm.

In order to characterize the rectifier circuit, a large signal characterization setup was configured (the details are reported in [55]). Fig. 22(a) represents the DC voltage versus current generated from the circuit for each input power level across a 240-Ohm load resistor. The data measured falls on a straight line, indicating that the diode rectifier is being driven in a forward and reverse direction by the incoming RF signal and has not reached the maximum limits of forward current and reverse breakdown voltage. Fig. 22(b) highlights the latter in detail, where the DC power generated by the circuit is shown as a function of the input power absorbed by the circuit. A fitted curve is also included to highlight what trajectory is expected for higher input power.

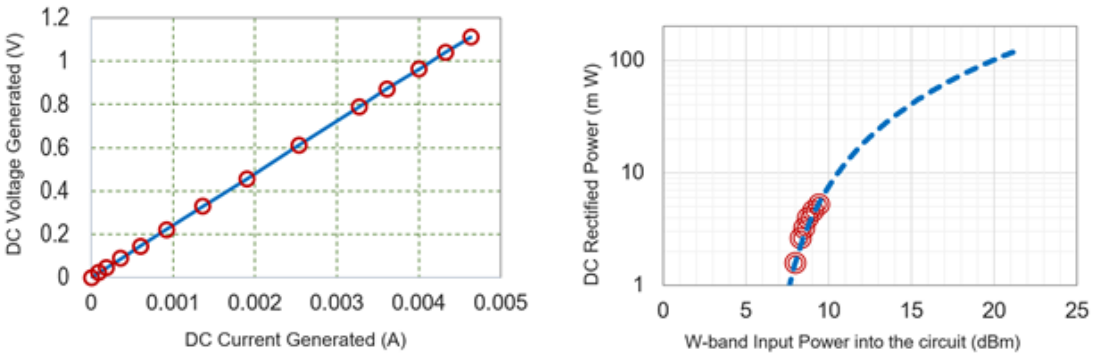

(a) (b)

Fig. 22. GaN nano-Schottly rectenna MMIC DC voltage versus current measured under a large signal at 93 GHz. Each data point indicates an input power level incident on the rectenna circuit. The lower plot highlights the DC power generated by the rectenna circuit versus incident power. The dotted line represents the higher power level trajectory if more power were available on the test system.

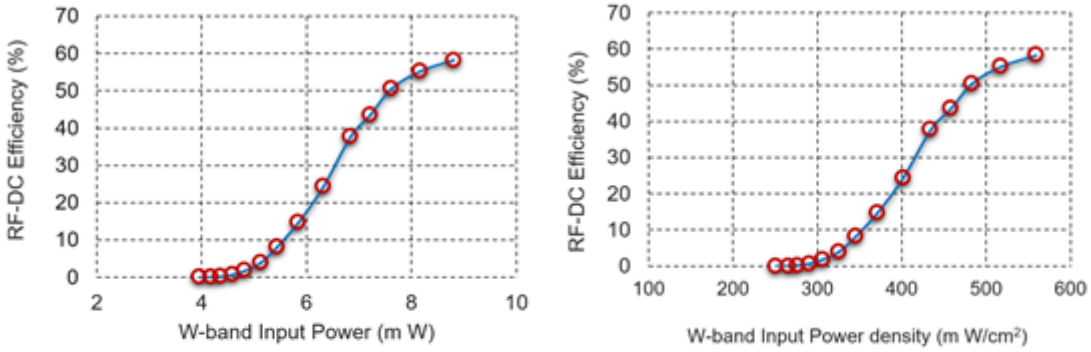

(a) (b)

Fig.23. The plots of RF-DC efficiency at 93 GHz are shown versus input power level and the power density.

The rectifier is connected to an antenna to form a rectenna. Fig. 23 represents the conversion efficiency plots for the measurements as a function of W-band input power absorbed by the circuit and the power density (power absorbed per unit area of the MMIC). The data represents the highest efficiency rectenna circuit reported at the W-band frequency range. It can be seen that the efficiency has not peaked completely and with more input power even higher values could be achieved. The input power density is also calculated as the ratio of the input power versus the area of the circuit MMIC. The value of 0.560 W/cm^2 indicates the highest power handling level of a W-band rectifier to date. A conversion efficiency of 61.5% was recorded during the high input power of 9.512 dBm, representing the highest reported millimeter wave rectifier efficiency at this power level. Table II represents the latest published W-band rectenna circuit performance metrics compared to the GaN-nano-Schottly rectenna circuit. Si CMOS circuits provide very high switching speeds but fall short on power handling due to the lower inherent breakdown voltage and current carrying capability of the diode rectifier. However, CMOS presents a high degree of integration and can provide substantial advantages for lower power arrays due to its many layers of interconnects and capability of integrating the power conditioning circuits. GaAs diodes, a predominant millimeter wave and sub-millimeter wave device technology, also provide great switching speeds and moderate breakdown voltage and hence

improvement over the silicon CMOS-based rectenna metrics. The GaN nano-Schottky rectenna circuits reported in this work shows an improvement of 1.5X in power handling over GaAs and 9.5X over CMOS rectenna circuits while improving the efficiency by 15.7% over the highest previously reported W-band rectenna circuits. Therefore, GaN nano-Schottky represents the next-generation technology for high-power mmWave wireless power beaming.

Reference	[56]	[57]	[58]	[59]	[60]	This WORK
Rectifier Tech.	GaAs Diode	0.13um CMOS Sch Diode	65nm CMOS	GaAs Diode	40nm CMOS	GaN nano Schottky
Architecture	Ant + Diode Chip	Integ MMIC with Ant	Integ MMIC with Ant	Ant + Diode Chip	MMIC no-Ant.	MMIC no-Ant
Tx Source Type	Klystron	Network Analyzer	Solid State Power Amp	Solid State Power Amp	Network Analyzer	Solid State Power Amp
Tx power (W)	100	0.1	014	0.4	0.063	0.09
Rectenna DC Power (mW)	0.65	0.9	0.1	39	0.029	5.7
Efficiency (%)	32.3	37	10	38	45.8	61.5
Element Area (mm^2)	5.62	2.9	0.48	18	0.0756	1.58
Power Handling (kW/m^2)	0.17	0.31	0.038	2.38	0.38	3.61

Table II. Comparative performance of various published rectenna circuits at 94-95 GHz.

Applications

Space-Based Solar Power

In the 1960s W. C. Brown first used narrow-beam microwaves as energy carriers [61]. However, at the time, commercial applications of narrow-beam WPT were limited, except for space applications, in particular space-based solar power (SBSP). P. E. Glaser proposed SBSP in 1968 [62] following Brown's success in 1964 with the first narrow-beam WPT experiment in a drone aircraft. However, theoretically, narrow-beam WPT requires large antennas, even in the case of microwaves, to increase beam efficiency. Hence, narrow-beam WPT has historically been viewed as economically infeasible and wired power transfer is still preferred. SBSP is the only exception to this rule.

Typical SBSP design parameters when used with microwaves are as follows (Fig. 24):

- Frequency: 5.8 GHz CW or 2.45 GHz CW
- Transmitting antenna: up to 2 km phased array with over 100 million elements
- Estimated beam efficiency: >90% at a distance of 36,000 km
- Received and rectified power on ground: 1 GW DC

Some SBSP systems are designed with laser power transfer. In the US, the Naval Research Laboratory recently demonstrated laser power transfer. The Department of Defence also launched a US $100 million partnership with Northrop Grumman, the Space Solar Power Incremental Demonstrations and Research Project (SSPIDR), which aims to launch an SBSP demonstration spacecraft called Arachne in 2024 [63]. Japan proposed a roadmap to commercial SBSP before 2050 by considering the required R&D steps and potential commercial spin-off WPT technologies. For example, in 2018, a narrow-beam WPT experiment was conducted on a drone with a phased array antenna at 5.8 GHz in Japan. WPT-assisted drones are one of the expected spin-off technologies [63]. Recently, China launched a national project for SBSP [64]. China plans to use a new superheavy lift rocket, which is currently under development, to construct a massive SBSP in the geostationary orbit. It is supported by a Chinese rocket company. China hopes to develop a megawatt-level power generation facility around 2030 [65]-[67]. The UK also initiated a feasibility study on SBSP as a CO_2-free source of power.

SBSP requires long distance and high efficiency beam WPT. Recently there are some interesting beam WPT being demonstrated in the world. In Japan, a high-efficiency and thin phased array antenna with a newly developed GaN HEMT was developed [63]. In 2015, they carried out 1.6kW - 50m distance narrow-beam WPT at 5.8GHz and succeeded in receiving 330W DC. Now they are developing a sandwich module with solar cells and a phased array antenna for space experiments in the near future. In the US, 91.2kW – 1km distance narrow beam WPT at 10.5GHz with a Cassegrain antenna succeeded in receiving 1.6kW DC in 2021[4]. Chinese researchers carried out 910W – 30m distance narrow beam WPT at 5.8GHz with a phased array antenna and succeeded in receiving 36W DC, also in 2021. Building on their successful development and demonstration of long-distance and high-efficiency WPT, all three countries-- Japan, the US, and China-- plan to carry out satellite experiments on SBSP.

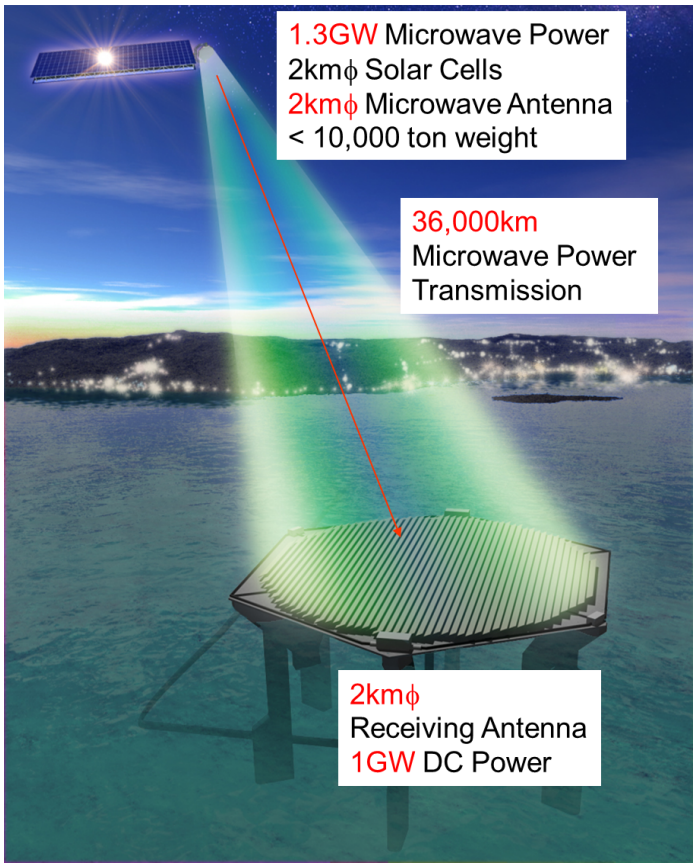

Fig.24. Typical image of SBSP with microwaves.

There are other WPT space applications in addition to SBSP. In the 1990s, a research group at Kyoto University in Japan designed a power satellite using 35-GHz WPT, which could supply wireless power to a user satellite (see Fig. 25) [68]. With such a power source, we can reduce the weight of a working satellite using lightweight rectennas instead of heavy solar cells and batteries.

WPT on the Moon is another interesting WPT application. We could power a Moon rover via microwave or millimeter wave wireless energy transfer. We could also supply wireless power to non-sunlit areas of the Moon's surface from a 100-km lunar orbit. This would bring us a step closer to practical SBSP and to achieving a new paradigm for space exploration.

Not only narrow-beam WPT but also wide-beam WPT and coupling WPT can be applied in space systems. The Internet of Space (IoS) based on wide-beam WPT is an important new concept in space system engineering. In small satellites, we can reduce the weight of power cables using inductive WPT. Overall, WPT shows novel potential to expand human space activities.

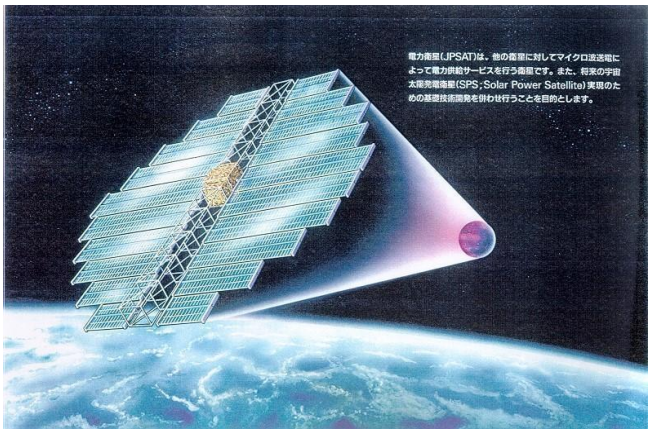

Fig. 25. Image of a power satellite.

SWIPT

In IoT networks, a challenge is to combine wireless powering with data communications, also called simultaneous wireless information and power transfer, or SWIPT (Fig. 26). The requirements are often contradictory, and therefore an optimal balance must be found between efficient wireless powering on the one hand, and reliable communications (i.e., low bit error rate (BER) and high data rate) on the other hand. As an example, the cut-off frequency of the low-pass filter of the rectifier should be as low as possible for optimal power harvesting, thus avoiding a ripple, while the ripple is essential for data communication as it contains the modulated information [32]. Thus, research on SWIPT focuses on two main aspects: the IoT node design, and the base station signal design [69][70].

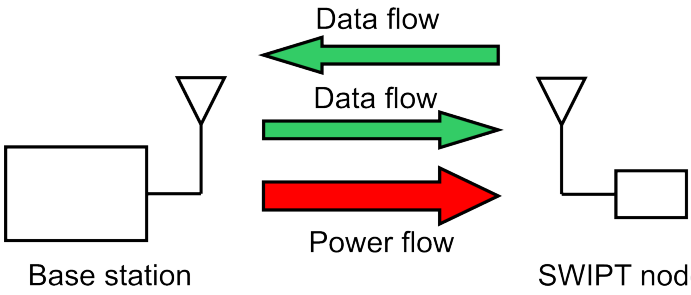

Fig. 26: In an IoT network, the base station would transmit both wireless power and data towards the IoT nodes, and receive the uplink data communications [72].

Various IoT node architectures have been explored (Fig. 27), and a promising one is the compact so-called “integrated” configuration, whereby the split between energy harvesting and information retrieval is not achieved at RF, but in the baseband. If the split were to happen at RF, an additional downconversion block would be required, and such additional RF oscillator-mixer topology increases the power requirements of the IoT node.

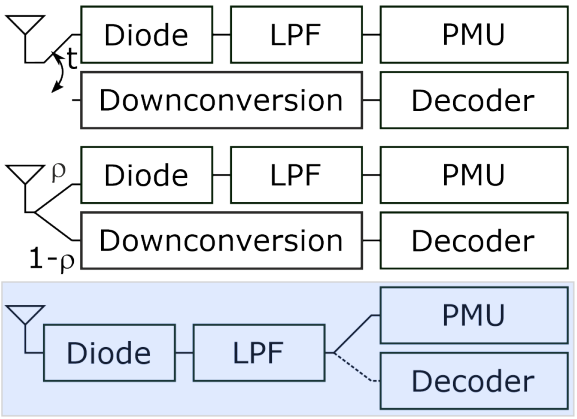

Fig. 27: Possible architectures for SWIPT IoT nodes: (top) time switching; (middle) power splitting; (bottom) integrated topology with data/energy split in the baseband.

Even though it is possible to harvest power from existing modulations adopted in IoT networks, such as Bluetooth Low Energy (BLE) [71], the performance is suboptimal in terms of power harvesting. Therefore, research is being conducted on novel modulation techniques that improve power conversion efficiency while minimizing the deterioration of the communication performance metrics (i.e., data rate, BER) for example, in [72],[73]. Besides the base station's waveform design, another degree of freedom to improve SWIPT performance is by exploiting the base station's antenna configuration, namely by adopting distributed antenna settings [74].

Medical Applications

Currently, most of the US Food and Drug Administration (FDA) approved medical implants that implement wireless power charging capability utilize inductive or resonance coupling by coils. They include neurostimulators that are implanted under the skin at the waist or chest, and cochlear implants behind the ear. The tissue distance is typically within a few millimeters and size of the implants are on the order of centimeters. Since the tissue thickness is fixed, the dielectric characteristics between the transmitter and implant coils are known, and the variations for wireless power efficiency depend solely on spatial misalignment of coils. The systems are operated in low MHz frequency ranges owing to the lower AC resistance.

For deeper tissues, the field divergence and misalignment issues become challenges. A miniature gastric stimulator attached to the stomach wall, which inevitably moves during digestion, can harvest sufficient power at 1.3 MHz through 7-cm thick tissues [75]. Field manipulation with spiral coils can give better power coverage to tolerate misalignment [76]. The field distributions cannot be modeled in an equivalent circuit. Finite-element simulations are needed to evaluate the available field strengths at a certain implant depth.

Mid-field power transfer techniques at higher MHz and lower GHz ranges have been proposed for millimeter-scale implants that are deeper in the body. Unwanted signals with higher frequencies attenuate faster in tissue, preventing interference; and a smaller antenna spatially reduces noise coupling into the electronics. However, the trade-offs highlight the need for better focusing of energy onto the implant via field manipulation.

An electrical stimulator with a 2-mm diameter and 2.5-mm length can be powered at a depth of 5 cm with a power of 500 mW at 1.6 GHz [77]. The transmitter metal pattern includes four split rings with

independent excitation ports to adjust phases, and a circular slot array to generate the desired current distributions. The fields converge on the implant with a measured power of 200 µW in phantoms. At a 10-cm depth, 10-µW of power can be received, which is comparable to the power consumption of a cardiac pacemaker.

A meandered-line patch antenna in a capsule-type implant receives 6.7-mW of power at a tissue thickness of 5 cm with 1-W of transmitting power [78]. The transmitter antenna contains four ports to control the phases for better radiation focusing. Dynamic phase adjustment gives operational flexibility to power the imaging capsule as it moves through the gastrointestinal tract.

Far-field power transfer has been demonstrated from a horn antenna with a 7.6-dBi gain to a subcutaneous implant with a 4x8 mm^2 inverted-F antenna at 2.45 GHz [79]. The transmitter power is limited to 1 W by safety rules. This technique can remotely charge the implant with ambient wireless energy; however, the efficiency may vary significantly due to the directivities between antennas.

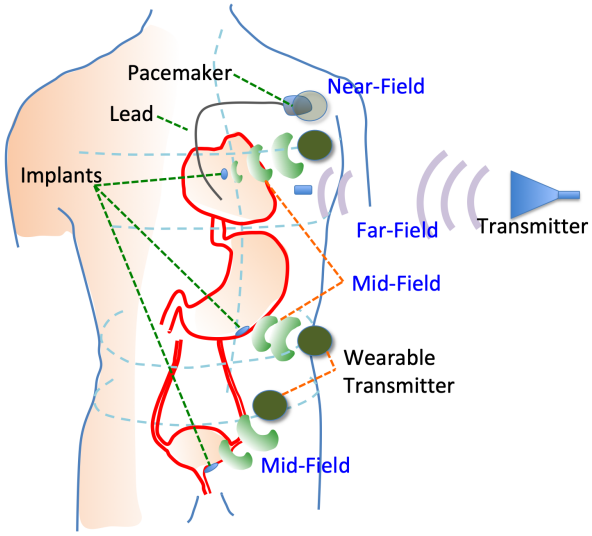

Fig. 28. Illustration of near-, mid-, and far-field wireless power transfer to implants.

For mid- and far-field power transfer systems, their implementation examples are illustrated in Fig. 28, as compared to the near-field, where coils are placed directly on top of the subcutaneous implant. For mid- and far-field systems, exposure limits to tissue generally follow the guidelines of IEEE C95.1 Standard [80] and ICNIRP Guidelines [81]. Absorption limits per unit weight of tissues are defined by specific absorption rate (SAR) and specific absorption (SA) to prevent thermal damage. IEEE C95.1 Standard limits the 10-g averaged SAR and SA for a 6-min time period to 1.6 W/kg and 576 J/kg, respectively. ICNIRP Guidelines limit the 10-g averaged SAR of the head to 2W/kg below 10 GHz and 2-mJ/kg averaged SA for a single pulse. Power flux densities for implants at different depths for 915 MHz and 2.4 and 5.8 GHz have been studied [82]. The methodologies for assessing exposure and anatomical models for dosimetry in wireless power transfer systems are discussed in [83].

Batteryless wireless sensors for structural health monitoring applications

The efficient design of wireless sensor networks (WSNs) including wireless battery-free sensor nodes (BFSNs) involves several key points that have to be simultaneously addressed at both the network and

the sensor levels, on hardware and software implementation. An example of a meshed wireless BFSN network topology designed for structural health monitoring applications in civil engineering is reported in [84], [85] and depicted in Fig. 29.

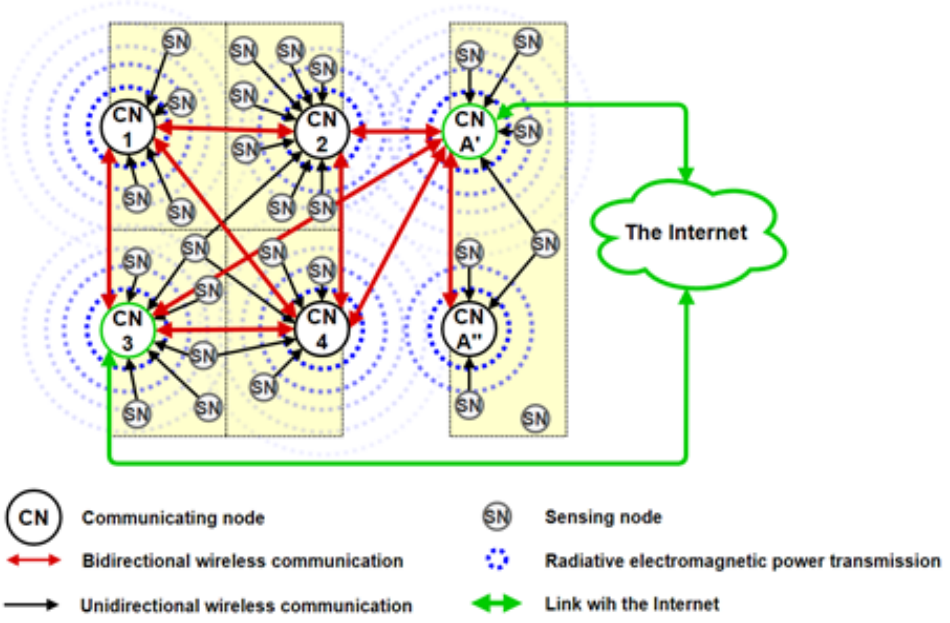

Fig. 29. Example of a network topology including wireless BFSNs. BFSNs are wirelessly powered using a far-field radiative WPT technique based on RF sources driven by the CNs.

The WSN represented in Fig. 29 is composed of two kinds of nodes: the communicating nodes (CNs) and the BFSNs. BFSNs are critical elements designed to be embedded in concrete for performing physical measurements (e.g., temperature and humidity) to enable the monitoring of civil engineering structures. In order to reduce the DC consumption of each BFSN, only a directional uplink communication (from BFSN to CN) was implemented. BFSNs are cold-start compatible and powered using a far-field radiative WPT technique from dedicated RF sources (operating at ISM 868 MHz) driven by a CN (and usually collocated with other CNs). As proof of concept, two BFSNs were prototyped: (i) a LoRa BFSN, represented in Fig. 30; and (ii) a BLE BFSN, represented in Fig. 31.

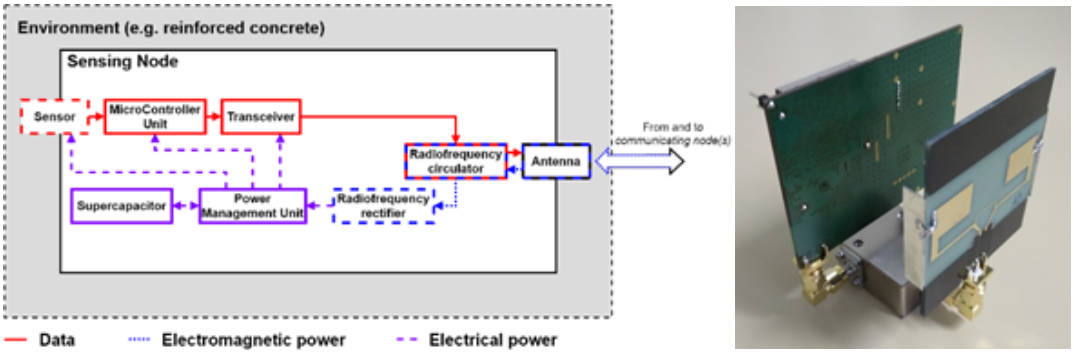

Fig. 30. Topology (left) and photo (right) of the LoRa BFSN.

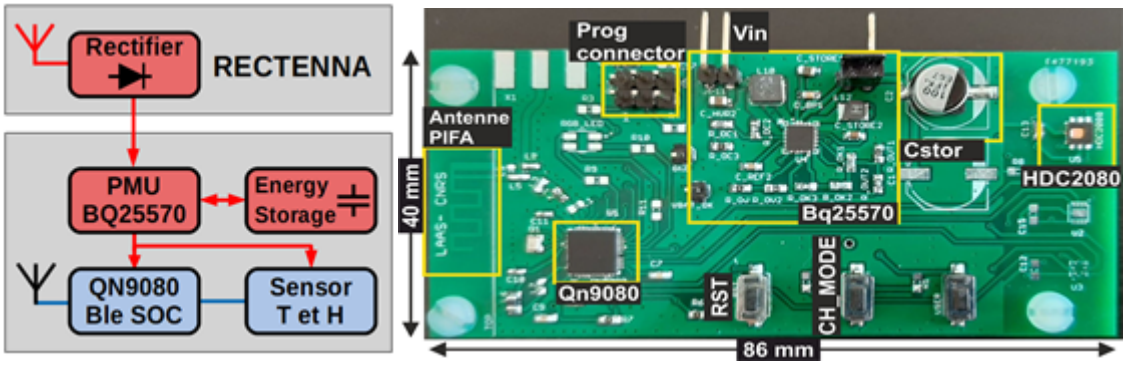

Fig. 31. Topology (left) and photo (right) of a manufactured prototype for the BLE BFSN. The external rectenna providing the DC power at the input V_{in} of the BLE BFSN is not represented here.

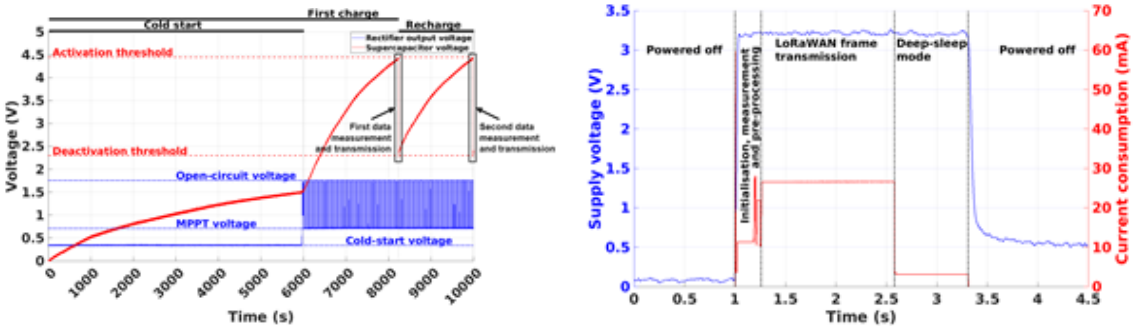

(a) (b)

Fig. 32. (a) Measured DC consumption for LoRa BFSN, (b) DC voltage at the port of the storage capacitor (22 mF) as a function of the performed task (experimental results obtained for a measured RF power of -5 dBm at the input of the RF rectifier).

As far as the topology, the wireless chipsets (Murata CMWX1ZZABZ-091 for the LoRa BFSN and NXP QN9080 for the BLE BFSN), the sensors (Texas Instruments HDC 2080), and the power management unit (Texas Instruments BQ25570) were selected; there are only a few ways to reduce the DC consumption of BFSN. A typical DC power consumption for the LoRa BFSN is represented in Fig. 32(a); while Fig. 32(b) highlights the evolution of the DC voltage of the storage capacitor (22 mF) as a function of the performed task.

For the LoRa BFSN, the DC consumption can be minimized by reducing the RF transmitting (Tx) power (DC current is reduced) and/or by increasing the data rate (thus decreasing the duration of the frame transmission). Both the Tx power and data rate are software controlled. Experimental results demonstrated that by reducing Tx power from +14 dBm to +4 dBm, the DC power consumption is reduced from 150 µW to 60 µW, while the energy/data byte is reduced from 52 mJ to 26.5 mJ. There is no practical interest in reducing the Tx power below +4 dBm because the communication range is highly impacted with a minimal gain in terms of energy/byte reduction. By increasing the data-rate from 250 bps to 5470 bps (Tx power: 4 dBm), the energy/data byte is reduced from 26.5 mJ to 5 mJ.

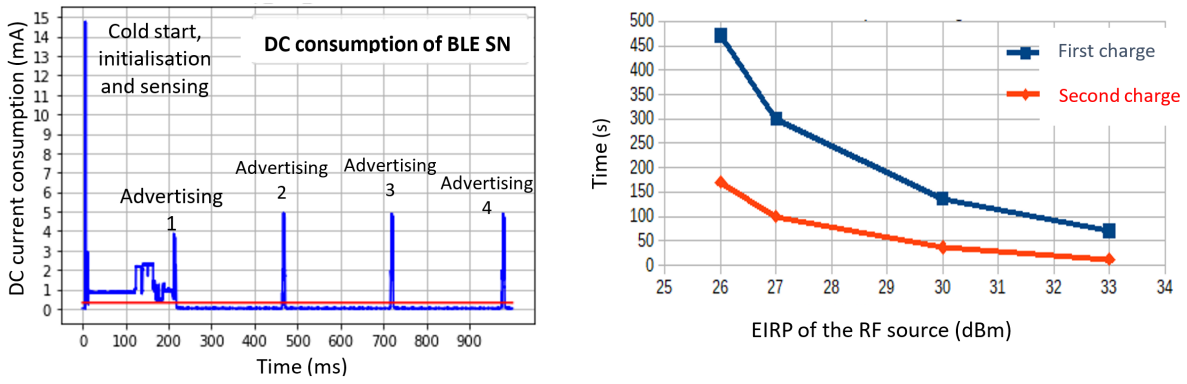

(a) (b)

Fig. 33. (a) Measured DC consumption for the BLE BFSN (DC voltage: 3V) for a complete frame transmission (red line is the average DC current), (b) duration of the first charge (including cold-start procedure) and of the second charge of the energy storage capacitor (100 µF) as a function of RF source EIRP.

For the BLE SN, the sensing data are sent to the CN over 4 start cycles (on each start, the same data frame is broadcast over BLE channels 37, 38, and 39). This high redundancy on the BLE SN side minimizes the probability of errors caused by potential interference, mainly with WiFi transmitters operating in roughly the same frequency band. The measured DC power consumption (Tx power: 0 dBm) is reported in Fig. 33(a). The measured first and second charging times of the storage capacitor (100 µF) as a function of the EIRP of the RF source is presented in Fig. 33(b). The measurements were performed in an anechoic chamber to avoid interference and multipath effects. The distance between the RF source and the BLE BFSN was fixed at 2 meters. The first physical measurement/sensing and transmission are performed after the first charge and the periodicity of sensing and transmission is the same as the duration of the second charge. These durations can be roughly controlled by controlling the EIRP of the RF source. The BLE BFSN implementation is more efficient than the LoRa BFSN implementation in terms of energy per transmitted frame (and per transmitted byte). Sending the data frame by BLE BFSN during one start cycle requires approximately 48 µJ (Tx power: 0 dBm) or about 1.2 mJ for a complete process, while the LoRa BFSN requires about 20 mJ for sending the data frame (Tx power: +4 dBm, data rate: 5470 bps). Better performance in terms of communication range in favor of the LoRa implementation justify this significant difference.

Two different SWIPT approaches were implemented. For the LoRa BFSN, the same antenna operating at 868 MHz in combination with a circulator was used for energy reception (from RF source) and data transmission (to CN). In the case of the BLE BFSN, two antennas were used: one operating at 868 MHz [86] for energy receiving and one operating at 2.45 GHz for data communication.

Conclusions

This paper has provided an overview of the current research progress on radiative WPT, describing where we are and where we want to go. Emerging research directions have been sketched, including

hybrid EH, mm-wave EH, and energy showers, which can improve the reliability and the versatility of the WPT approach. Diverse applications of radiative WPT have been reported as well, from medical, to space, to structural health monitoring. All this shows the potential and the positive impact that can be produced by radiative WPT on a growing number of application scenarios, and its key role in the evolution of the IoT.

References

[1] F. Boccardi, R. W. Heath, A. Lozano, T. L. Marzetta, and P. Popovski, "Five disruptive technology directions for 5G," IEEE Communications Magazine, 52, 2, Feb. 2014, pp. 74-80.

[2] CEPT Electronic Communications Committee, “ERC Recommendation 70-03”. [Online] Available: https://docdb.cept.org/download/25c41779-cd6e/Rec7003e.pdf.

[3] C. Song, P. Lu and S. Shen, "Highly Efficient Omnidirectional Integrated Multiband Wireless Energy Harvesters for Compact Sensor Nodes of Internet-of-Things," in IEEE Transactions on Industrial Electronics, vol. 68, no. 9, pp. 8128-8140, Sept. 2021.

[4] C. T. Rodenbeck *et al*., "Terrestrial Microwave Power Beaming," in *IEEE Journal of Microwaves*, vol. 2, no. 1, pp. 28-43, Jan. 2022.

[5] M. Wagih, A. S. Weddell and S. Beeby, "Omnidirectional Dual-Polarized Low-Profile Textile Rectenna With Over 50% Efficiency for Sub-µW/cm2 Wearable Power Harvesting," in IEEE Transactions on Antennas and Propagation, vol. 69, no. 5, pp. 2522-2536, May 2021.

[6] V. Palazzi, M. Del Prete and M. Fantuzzi, "Scavenging for Energy: A Rectenna Design for Wireless Energy Harvesting in UHF Mobile Telephony Bands," in IEEE Microwave Magazine, vol. 18, no. 1, pp. 91-99, Jan.-Feb. 2017.

[7] V. Palazzi et al., "A Novel Ultra-Lightweight Multiband Rectenna on Paper for RF Energy Harvesting in the Next Generation LTE Bands," in IEEE Transactions on Microwave Theory and Techniques, vol. 66, no. 1, pp. 366-379, Jan. 2018.

[8] P. D. Hilario Re, S. K. Podilchak, S. A. Rotenberg, G. Goussetis and J. Lee, "Circularly Polarized Retrodirective Antenna Array for Wireless Power Transmission," in IEEE Transactions on Antennas and Propagation, vol. 68, no. 4, pp. 2743-2752, April 2020.

[9]J. A. Hagerty, F. B. Helmbrecht, W. H. McCalpin, R. Zane and Z. B. Popovic, "Recycling ambient microwave energy with broad-band rectenna arrays," in IEEE Transactions on Microwave Theory and Techniques, vol. 52, no. 3, pp. 1014-1024, March 2004.

[10] C. Liu, H. Lin, Z. He and Z. Chen, "Compact Patch Rectennas Without Impedance Matching Network for Wireless Power Transmission," in *IEEE Transactions on Microwave Theory and Techniques*, vol. 70, no. 5, pp. 2882-2890, May 2022.

[11] G. Monti, L. Corchia and L. Tarricone, "UHF Wearable Rectenna on Textile Materials," in IEEE Transactions on Antennas and Propagation, vol. 61, no. 7, pp. 3869-3873, July 2013.

[12] D. Vital, S. Bhardwaj and J. L. Volakis, "Textile-Based Large Area RF-Power Harvesting System for Wearable Applications," in IEEE Transactions on Antennas and Propagation, vol. 68, no. 3, pp. 2323-2331, March 2020.

[13] R. Scheeler, S. Korhummel and Z. Popovic, "A Dual-Frequency Ultralow-Power Efficient 0.5-g Rectenna," in IEEE Microwave Magazine, vol. 15, no. 1, pp. 109-114, Jan.-Feb. 2014.

[14] J. Kimionis, M. Isakov, B. S. Koh, A. Georgiadis and M. M. Tentzeris, "3D-Printed Origami Packaging With Inkjet-Printed Antennas for RF Harvesting Sensors," in IEEE Transactions on Microwave Theory and Techniques, vol. 63, no. 12, pp. 4521-4532, Dec. 2015.

[15] Ricardo Correia, "Passive backscatter wireless sensor with wireless power transmission for IoT applications", PhD Thesis, DETI - Departamento de Eletrónica, Telecomunicações e Informática, Aveiro, Portugal. [Online] Available: https://ria.ua.pt/handle/10773/29173.

[16] Y. Suh and K. Chang, "A High-Efficiency Dual-Frequency Rectenna for 2.45- and 5.8-GHz Wireless Power Transmission," IEEE Trans. Microw. Theory Tech., vol. 50, no. 7, pp.1784–1789, 2002.

[17] B. L. Pham and A.-V. Pham, "Triple bands antenna and high efficiency rectifier design for RF energy harvesting at 900, 1900 and 2400 MHz," in 2013 IEEE MTT-S Int. Microw. Symp. Dig. IEEE, Jun 2013, pp. 1–3.

[18] Z. Zhong, H. Sun, and Y. Guo, "Design of rectifier with extended operating input power range," Electron. Lett., vol. 49, no. 18, pp. 1175–1176, Aug 2013.

[19] R. Correia and N. B. Carvalho, "Single transistor passive backscatter sensor," in 2017 IEEE MTT-S Int. Microw. Symp. IEEE, Jun 2017, pp. 820–823.

[20] C. Wang, B. Yang and N. Shinohara, "Study and Design of a 2.45-GHz Rectifier Achieving 91% Efficiency at 5-W Input Power," in *IEEE Microwave and Wireless Components Letters*, vol. 31, no. 1, pp. 76-79, Jan. 2021.

[21] H. Sun, Z. Zhong, and Y.-X. Guo, "An Adaptive Reconfigurable Rectifier for Wireless Power Transmission," IEEE Microw. Wirel. Components Lett., vol. 23, no. 9, pp. 492–494, Sep 2013.

[22] C. R. Valenta and G. D. Durgin, "Harvesting Wireless Power: Survey of Energy-Harvester Conversion Efficiency in Far-Field,Wireless Power Transfer Systems," IEEE Microw. Mag., vol. 15, no. 4, pp. 108–120, Jun 2014.

[23]. F. Zhao, D. Inserra, G. Gao, Y. Huang, J. Li and G. Wen, "High-Efficiency Microwave Rectifier With Coupled Transmission Line for Low-Power Energy Harvesting and Wireless Power Transmission," in IEEE Transactions on Microwave Theory and Techniques, vol. 69, no. 1, pp. 916-925, Jan. 2021.

[24] Z. He, J. Lan and C. Liu, "Compact Rectifiers With Ultra-wide Input Power Range Based on Nonlinear Impedance Characteristics of Schottky Diodes," in *IEEE Transactions on Power Electronics*, vol. 36, no. 7, pp. 7407-7411, July 2021.

[25] N. Sakai, K. Noguchi and K. Itoh, "A 5.8-GHz Band Highly Efficient 1-W Rectenna With Short-Stub-Connected High-Impedance Dipole Antenna," in IEEE Transactions on Microwave Theory and Techniques, vol. 69, no. 7, pp. 3558-3566, July 2021.

[26] M. Trotter, J. Griffin, and G. Durgin, “Power-optimized waveforms for improving the range and reliability of RFID systems,” in 2009 IEEE Int. Conf. RFID. IEEE, Apr 2009, pp. 80–87.

[27] S. A. Rotenberg, S. K. Podilchak, P. D. H. Re, C. Mateo-Segura, G. Goussetis and J. Lee, "Efficient Rectifier for Wireless Power Transmission Systems," in IEEE Transactions on Microwave Theory and Techniques, vol. 68, no. 5, pp. 1921-1932, May 2020.

[28] A. S. Boaventura and N. B. Carvalho, “Maximizing DC power in energy harvesting circuits using multisine excitation,” in 2011 IEEE MTT-S Int. Microw. Symp. IEEE, Jun 2011, pp. 1–4.

[29] A. Collado and A. Georgiadis, “Improving wireless power transmission efficiency using chaotic waveforms,” in 2012 IEEE/MTT-S Int. Microw. Symp. Dig. IEEE, Jun 2012, pp. 1–3.

[30] A. Boaventura, D. Belo, R. Fernandes, A. Collado, A. Georgiadis, and N. B. Carvalho, “Boosting the Efficiency: Unconventional Waveform Design for Efficient Wireless Power Transfer,” IEEE Microw. Mag., vol. 16, no. 3, pp. 87–96, Apr 2015.

[31] C. R. Valenta and G. D. Durgin, “Rectenna performance under power-optimized waveform excitation,” in 2013 IEEE Int. Conf. RFID. IEEE, Apr 2013, pp. 237–244.

[32] N. Pan, D. Belo, M. Rajabi, D. Schreurs, N. B. Carvalho, and S. Pollin, “Bandwidth Analysis of RF-DC Converters Under Multisine Excitation,” IEEE Trans. Microw. Theory Tech., vol. 66, no. 2, pp. 791–802, Feb 2018.

[33] J. Blanco, F. Bolos, and A. Georgiadis, “Instantaneous power variance and radio frequency to dc conversion efficiency of wireless power transfer systems,” IET Microwaves, Antennas Propag., vol. 10, no. 10, pp. 1065–1070, Jul 2016.

[34] X. Gu, P. Burasa, S. Hemour, and K. Wu, "Recycling ambient rf energy: Far-field wireless power transfer and harmonic backscattering," *IEEE Microw. Mag.*, vol. 22, no. 9, pp. 60-78, Sept. 2021.

[35] S. Hemour, et al., "Towards low-power high-efficiency rf and microwave energy harvesting," *IEEE Trans. Microw. Theory Techn.*, vol. 62, no. 4, pp. 965-976, Apr. 2014.

[36] X. Gu, S. Hemour, and K. Wu, "Far-field wireless power harvesting: Nonlinear modeling, rectenna design, and emerging applications," *Proc. IEEE*, vol. 110, no. 1, pp. 56-73, Jan. 2022.

[37] E. Fazzini, A. Costanzo and D. Masotti, "Range Selective Power Focusing with Time-controlled Bi-dimensional Frequency Diverse Arrays," 2021 IEEE Wireless Power Transfer Conference (WPTC), 2021, pp. 1-4.

[38] D. Masotti, A. Costanzo, M. Del Prete and V. Rizzoli, "Time-Modulation of Linear Arrays for Real-Time Reconfigurable Wireless Power Transmission," in IEEE Transactions on Microwave Theory and Techniques, vol. 64, no. 2, pp. 331-342, Feb. 2016.

[39] Goldsmith, P. F.: Quasioptical Systems: Gaussian Beam Quasioptical Propagation and Applications, IEEE Press, Piscataway, NJ, 1998.

[40] Pereira, R., Carvalho, N., & Da Cunha, J. (2018). Quasi-optical analysis of a double reflector microwave antenna system. Wireless Power Transfer, 5(2), 75-86. doi:10.1017/wpt.2017.19.

[41] R. A. M. Pereira, N. B. Carvalho and A. Georgiadis, "Focus Location Measurement of a Quasioptical Double Reflector System," 2021 IEEE Wireless Power Transfer Conference (WPTC), 2021, pp. 1-4, doi: 10.1109/WPTC51349.2021.9457870.

[42] David R. Smith, Vinay R. Gowda, Okan Yurduseven, Stéphane Larouche, Guy Lipworth, Yaroslav Urzhumov, and Matthew S. Reynolds, "An analysis of beamed wireless power transfer in the Fresnel zone using a dynamic, metasurface aperture", Journal of Applied Physics 121, 014901 (2017), https://doi.org/10.1063/1.4973345

[43] A. Georgiadis, A. Collado and M. M. Tentzeris, Energy Harvesting, Technologies, Systems and Challenges, Cambridge University Press, 2021.

[44] A. Georgiadis, "Energy harvesting for autonomous wireless sensors and RFID's,'' in Proc. XXXIth URSI General Assembly and Scientific Symposium (URSI GASS), Beijing, 2014, pp. 1-5.

[45] H. J. Visser, A. Reniers, and J. Theeuwes, "Ambient RF energy scavenging: GSM and WLAN power density measurements,'' in Proc. European Microwave Conference, Amsterdam, 2008.

[46] Y. Kawahara, K. Tsukada, and T. Asami, "Feasibility and potential application of power scavenging from environmental RF signals,'' in Proc. IEEE AP-S Antennas and Propagation International Symposium (APSURSI), Charleston, 2009.

[47] R. J. Vyas, B. S. Cook, Y. Kawahara, and M. M. Tentzeris, "E-WEHP: A batteryless embedded sensor-platform wirelessly powered from ambient digital-TV signals,'' IEEE Transactions on Microwave Theory and Techniques, 61 ,6, June 2013, pp. 2491-2505.

[48] R. J. Gutmann and J. M. Borrego, "Power Combining in an Array of Microwave Power Rectifiers," in IEEE Transactions on Microwave Theory and Techniques, vol. 27, no. 12, pp. 958-968, Dec. 1979, doi: 10.1109/TMTT.1979.1129774.

[49] A. Georgiadis, "Energy harvesting for autonomous wireless sensor platforms,'' in Proc. XXXIVth URSI General Assembly and Scientific Symposium (URSI GASS), Rome, 2021, pp. 1-3.

[50] M. Virili, A. Georgiadis, A. Collado, P. Mezzanotte, and L. Roselli, "EM characterization of a patch antenna with thermo-electric generator and solar cell for hybrid energy harvesting,'' in Proc. IEEE Radio and Wireless Symposium (RWS), San Diego, 2015, pp. 44-46.

[51] A. P. Sample, J. Braun, A. Parks and J. R. Smith, "Photovoltaic enhanced UHF RFID tag antennas for dual purpose energy harvesting," 2011 IEEE International Conference on RFID, 2011, pp. 146-153.

[52] A. Georgiadis and A. Collado, "Improving range of passive RFID tags utilizing energy harvesting and high efficiency class-E oscillators,'' in Proc. 6th European Conference on Antennas and Propagation (EuCAP), Prague, 2012, pp. 3455-3458.

[53] V. Liu, A. Parks, V. Talla, S. Gollakota, D. Wetherall, and J. R. Smith, "Ambient backscatter: wireless communication out of thin air,'' in Proc. ACM SIGCOMM, 2013, pp. 39-50.

[54] S. N. Daskalakis, J. Kimionis, A. Collado, G. Goussetis, M. M. Tentzeris, and A. Georgiadis, "Ambient backscatterers using FM broadcasting for low cost and low power wireless applications,'' IEEE Transactions on Microwave Theory and Techniques, 65, 12, Dec. 2017, pp. 5251-5262.

[55] H. Kazemi, "61.5% Efficiency and 3.6 kW/m² Power Handling Rectenna Circuit Demonstration for Radiative Millimeter Wave Wireless Power Transmission," in IEEE Transactions on Microwave Theory and Techniques, Vol. 70, issue 1, Jan 2022, pp. 650-658.

[56] S. Hemour, C. H. P. Lorenz, and K. Wu, “Small-footprint wideband 94 GHz rectifier for swarm micro-robotics,” in IEEE MTT-S Int. Microw. Symp. Dig., May 2015, pp. 1–4.

[57] H.-K. Chiou and I.-S. Chen, “High-efficiency dual-band on-chip rectenna for 35- and 94-GHz wireless power transmission in 0.13-µm CMOS technology,” IEEE Trans. Microw. Theory Techn., vol. 58, no. 12, pp. 3598–3606, Dec. 2010.

[58] N. Weissman, S. Jameson, and E. Socher, “W-band CMOS on-chip energy harvester and rectenna,” in IEEE MTT-S Int. Microw. Symp. Dig., Tampa, FL, USA, Jun. 2014, pp. 1–6.

[59] K. Matsui et al., “Microstrip antenna and rectifier for wireless power transfer at 94 GHz,” in Proc. IEEE Wireless Power Transf. Conf. (WPTC), Taipei, Taiwan, May 2017, pp. 1–3.

[60] P. He, J. Xu, and D. Zhao, “A W-band rectenna using on-chip CMOS switching rectifier and on-PCB tapered slot antenna achieving 25% effective-power-conversion efficiency for wireless power transfer,” in IEEE MTT-S Int. Microw. Symp. Dig., Aug. 2020, pp. 1055–1058.

[61] Brown, W. C., “The History of Power Transmission by Radio Waves,” IEEE Trans. MTT, Vol. 32, No. 9, pp.1230-1242, 1984.

[62] Glaser, P. E., “Power from the Sun,” Science, No.162, pp.857-886, 1968.

[63] Rodenbeck, C. T., P. I. Jaffe, B. H. Strassner II, P. E. Hausgen, J. O. McSpadden, H. Kazemi, N. Shinohara, B. B. Tierney, C. B. DePuma, and A. P. Self, “Microwave and Millimeter Wave Power Beaming,” IEEE Journal of Microwave, vol.1, no.1, pp.229-259, 2021.

[64] Shinohara, N., “Recent Advance of Beam Wireless Power Transfer for Solar Power Satellite in Japan,” IEEE Wireless Power Week 2021 School, San Diego, US, and Online, 2021.6.1 (on YouTube https://www.youtube.com/watch?v=JLVx56c9_30”.

[65] “China to build space-based solar power station by 2035”. [Online] Available: https://english.www.gov.cn/news/topnews/201912/02/content_WS5de47b72c6d0bcf8c4c182a1.html.

[66] “China’s super heavy rocket to construct space-based solar power station" by Andrew Jones — June 28, 2021. [Online] Available: https://spacenews.com/chinas-super-heavy-rocket-to-construct-space-based-solar-power-station.

[67] HOU Xinbin, WANG Li, “Study on Multi-Rotary Joints Space Power Satellite Concept,” Aerospace China, 2018, Vol. 19, Issue (1): 19-26.

[68] Matsumoto, H., N. Kaya, S. Kinai, T. Fujiwara, and J. Kochiyama, “A Feasibility study of power supplying satellite (PSS),” Space Power, No.12, pp.1-6, 1993.

[69] B. Clerckx, R. Zhang, R. Schober, D. W. K. Ng, D. I. Kim and H. V. Poor, "Fundamentals of Wireless Information and Power Transfer: From RF Energy Harvester Models to Signal and System Designs," in IEEE Journal on Selected Areas in Communications, vol. 37, no. 1, pp. 4-33, Jan. 2019.

[70] A. Costanzo, D. Masotti, G. Paolini and D. Schreurs, "Evolution of SWIPT for the IoT World: Near- and Far-Field Solutions for Simultaneous Wireless Information and Power Transfer," in IEEE Microwave Magazine, vol. 22, no. 12, pp. 48-59, Dec. 2021.

[71] G. Paolini et al., "RF Energy Harvesting from GFSK-Modulated BLE Signals," IEEE Topical Conference on Wireless Sensors and Sensor Networks (WiSNeT), 2021, pp. 27-29.

[72] M. Rajabi, N. Pan, S. Claessens, S. Pollin and D. Schreurs, "Modulation Techniques for Simultaneous Wireless Information and Power Transfer with an Integrated Rectifier–Receiver," IEEE Transactions on Microwave Theory and Techniques, vol. 66, no. 5, pp. 2373-2385, May 2018.

[73] S. Claessens, N. Pan, D. Schreurs and S. Pollin, "Multitone FSK Modulation for SWIPT," IEEE Transactions on Microwave Theory and Techniques, vol. 67, no. 5, pp. 1665-1674, May 2019.

[74] S. Shen, J. Kim, C. Song and B. Clerckx, "Wireless Power Transfer with Distributed Antennas: System Design, Prototype, and Experiments," IEEE Transactions on Industrial Electronics, vol. 68, no. 11, pp. 10868-10878, Nov. 2021.

[75] S. Deb, S. Tang, T.L. Abell, S. Rao, W. Huang, S.F. To, C. Lahr and J. Chiao, "An endoscopic wireless gastrostimulator," Gastrointest. Endosc., vol. 75, pp. 411-415. 2012.

[76] M.Q. Nguyen, Z. Hughes, P. Woods, Y. Seo, S. Rao and J. Chiao, "Field distribution models of spiral coil for misalignment analysis in wireless power transfer systems," IEEE Trans. Microwave Theory Tech., vol. 62, pp. 920-930, 2014.

[77] J.S. Ho, A.J. Yeh, E. Neofytou, S. Kim, Y. Tanabe, B. Patlolla, R.E. Beygui and A.S. Poon, "Wireless power transfer to deep-tissue microimplants," Proceedings of the National Academy of Sciences, vol. 111, pp. 7974-7979, 2014.

[78] A. Basir and H. Yoo, "Efficient wireless power transfer system with a miniaturized quad-band implantable antenna for deep-body multitasking implants," IEEE Trans. Microwave Theory Tech., vol. 68, pp. 1943-1953, 2020.

[79] C. Liu, Y. Guo, H. Sun and S. Xiao, "Design and safety considerations of an implantable rectenna for far-field wireless power transfer," IEEE Transactions on Antennas and Propagation, vol. 62, pp. 5798-5806, 2014.

[80] IEEE C95. 1, "IEEE Standard for Safety Levels with Respect to Human Exposure to Electric, Magnetic, and Electromagnetic Fields, 0 Hz to 300 GHz," 2019.

[81] International Commission on Non-Ionizing Radiation Protection, "ICNIRP guidelines on limiting exposure to time-varying electric, magnetic and electromagnetic fields (100 kHz to 300 GHz)," 2020.

[82] R.A. Bercich, D.R. Duffy and P.P. Irazoqui, "Far-field RF powering of implantable devices: Safety considerations," IEEE Transactions on Biomedical Engineering, vol. 60, pp. 2107-2112, 2013.

[83] A. Christ, M. Douglas, J. Nadakuduti and N. Kuster, "Assessing human exposure to electromagnetic fields from wireless power transmission systems," Proc. IEEE, vol. 101, pp. 1482-1493, 2013.

[84] G. Loubet, A. Takacs, and D. Dragomirescu, "Implementation of a Battery-Free Wireless Sensor for Cyber-Physical Systems Dedicated to Structural Health Monitoring Applications," in IEEE Access, vol. 7, pp. 24679-24690, 2019.

[85] G. Loubet, "Autonomous wireless sensor networks for the implementation of communicating materials. Application to civil engineering industry.," Doctoral dissertation, INSA Toulouse, 2021.

[86] A. Sidibe, A. Takacs, G. Loubet, and D. Dragomirescu, "Compact Antenna in 3D Configuration for Rectenna Wireless Power Transmission Applications," Sensors, vol. 21, no. 9, p. 3193, May 2021.